NOAA TECHNICAL MEMORANDUM
NWS WR-246

A WESTERN REGION GUIDE TO THE ETA-29 MODEL

Mike Staudenmaier, Jr.
Western Region SSD/NWSFO SLC
Salt Lake City, UT

March 1997

U.S. DEPARTMENT OF COMMERCE
National Oceanic and Atmospheric Administration
National Weather Service

NOAA TECHNICAL MEMORANDA
National Weather Service, Western Region Subseries

The National Weather Service (NWS) Western Region (WR) Subseries provides an informal medium for the documentation and quick dissemination of results not appropriate, or not yet ready, for formal publication. The series is used to report on work in progress, to describe technical procedures and practices, or to relate progress to a limited audience. These Technical Memoranda will report on investigations devoted primarily to regional and local problems of interest mainly to personnel, and hence will not be widely distributed.

Papers 1 to 25 are in the former series, ESSA Technical Memoranda, Western Region Technical Memoranda (WRTM); papers 24 to 59 are in the former series, ESSA Technical Memoranda, Weather Bureau Technical Memoranda (WBTM). Beginning with 60, the papers are part of the series, NOAA Technical Memoranda NWS. Out-of-print memoranda are not listed.

Papers 2 to 22, except for 5 (revised edition), are available from the National Weather Service Western Region, Scientific Services Division, 125 South State Street - Rm 1210, Salt Lake City, Utah 84138-1102. Paper 5 (revised edition), and all others beginning with 25 are available from the National Technical Information Service, U.S. Department of Commerce, Sills Building, 5285 Port Royal Road, Springfield, Virginia 22161. Prices vary for all paper copies; microfiche are $3.50. Order by accession number shown in parentheses at end of each entry.

ESSA Technical Memoranda (WRTM)

2 Climatological Precipitation Probabilities. Compiled by Lucianne Miller, December 1965.
3 Western Region Pre- and Post-FP-3 Program, December 1, 1965, to February 20, 1966. Edward D. Diemer, March 1966.
5 Station Descriptions of Local Effects on Synoptic Weather Patterns. Philip Williams, Jr., April 1966 (Revised November 1967, October 1969). (PB-17800)
8 Interpreting the RAREP. Herbert P. Benner, May 1966 (Revised January 1967).
11 Some Electrical Processes in the Atmosphere. J. Latham, June 1966.
17 A Digitalized Summary of Radar Echoes within 100 Miles of Sacramento, California. J. A. Youngberg and L. B. Overaas, December 1966.
21 An Objective Aid for Forecasting the End of East Winds in the Columbia Gorge, July through October. D. John Coparanis, April 1967.
22 Derivation of Radar Horizons in Mountainous Terrain. Roger G. Pappas, April 1967.

ESSA Technical Memoranda, Weather Bureau Technical Memoranda (WBTM)

25 Verification of Operation Probability of Precipitation Forecasts, April 1966-March 1967. W. W. Dickey, October 1967. (PB-176240)
26 A Study of Winds in the Lake Mead Recreation Area. R. P. Augulis, January 1968. (PB-177830)
28 Weather Extremes. R. J. Schmidli, April 1968 (Revised March 1986). (PB86 177672/AS). (Revised October 1991 - PB92-115062/AS)
29 Small-Scale Analysis and Prediction. Philip Williams, Jr., May 1968. (PB178425)
30 Numerical Weather Prediction and Synoptic Meteorology. CPT Thomas D. Murphy, USAF, May 1968. (AD 673365)
31 Precipitation Detection Probabilities by Salt Lake ARTC Radars. Robert K. Belesky, July 1968. (PB 179084)
32 Probability Forecasting--A Problem Analysis with Reference to the Portland Fire Weather District. Harold S. Ayer, July 1968. (PB 179289)
36 Temperature Trends in Sacramento--Another Heat Island. Anthony D. Lentini, February 1969. (PB 183055)
37 Disposal of Logging Residues Without Damage to Air Quality. Owen P. Cramer, March 1969. (PB 183057)
39 Upper-Air Lows Over Northwestern United States. A.L. Jacobson, April 1969. PB 184296)
40 The Man-Machine Mix in Applied Weather Forecasting in the 1970s. L.W. Snellman, August 1969. (PB 185068)
43 Forecasting Maximum Temperatures at Helena, Montana. David E. Olsen, October 1969. (PB 185762)
44 Estimated Return Periods for Short-Duration Precipitation in Arizona. Paul C. Kangieser, October 1969. (PB 187763)
46 Applications of the Net Radiometer to Short-Range Fog and Stratus Forecasting at Eugene, Oregon. L. Yee and E. Bates, December 1969. (PB 190476)
47 Statistical Analysis as a Flood Routing Tool. Robert J.C. Burnash, December 1969. (PB 188744)
48 Tsunami. Richard P. Augulis, February 1970. (PB 190157)
49 Predicting Precipitation Type. Robert J.C. Burnash and Floyd E. Hug, March 1970. (PB 190962)
50 Statistical Report on Aeroallergens (Pollens and Molds) Fort Huachuca, Arizona, 1969. Wayne S. Johnson, April 1970. (PB 191743)
51 Western Region Sea State and Surf Forecaster's Manual. Gordon C. Shields and Gerald B. Burdwell, July 1970. (PB 193102)
52 Sacramento Weather Radar Climatology. R.G. Pappas and C. M. Veliquette, July 1970. (PB 193347)
54 A Refinement of the Vorticity Field to Delineate Areas of Significant Precipitation. Barry B. Aronovitch, August 1970.
55 Application of the SSARR Model to a Basin without Discharge Record. Vail Schermerhorn and Donal W. Kuehl, August 1970. (PB 194394)
56 Areal Coverage of Precipitation in Northwestern Utah. Philip Williams, Jr., and Werner J. Heck, September 1970. (PB 194389)
57 Preliminary Report on Agricultural Field Burning vs. Atmospheric Visibility in the Willamette Valley of Oregon. Earl M. Bates and David O. Chilcote, September 1970. (PB 194710)
58 Air Pollution by Jet Aircraft at Seattle-Tacoma Airport. Wallace R. Donaldson, October 1970. (COM 71 00017)
59 Application of PE Model Forecast Parameters to Local-Area Forecasting. Leonard W. Snellman, October 1970. (COM 71 00016)
60 An Aid for Forecasting the Minimum Temperature at Medford, Oregon, Arthur W. Fritz, October 1970. (COM 71 00120)
63 700-mb Warm Air Advection as a Forecasting Tool for Montana and Northern Idaho. Norris E. Woerner, February 1971. (COM 71 00349)
64 Wind and Weather Regimes at Great Falls, Montana. Warren B. Price, March 1971.
65 Climate of Sacramento, California. Richard Honton and Tony Martini (Retired), August 1996. (Fifth Revision) (PB89 207781/AS)
66 A Preliminary Report on Correlation of ARTCC Radar Echoes and Precipitation. Wilbur K. Hall, June 1971. (COM 71 00829)
69 National Weather Service Support to Soaring Activities. Ellis Burton, August 1971. (COM 71 00956)
71 Western Region Synoptic Analysis-Problems and Methods. Philip Williams, Jr., February 1972. (COM 72 10433)
74 Thunderstorms and Hail Days Probabilities in Nevada. Clarence M. Sakamoto, April 1972. (COM 72 10554)
75 A Study of the Low Level Jet Stream of the San Joaquin Valley. Ronald A. Willis and Philip Williams, Jr., May 1972. (COM 72 10707)
76 Monthly Climatological Charts of the Behavior of Fog and Low Stratus at Los Angeles International Airport. Donald M. Gales, July 1972. (COM 72 11140)
77 A Study of Radar Echo Distribution in Arizona During July and August. John E. Hales, Jr., July 1972. (COM 72 11136)
78 Forecasting Precipitation at Bakersfield, California, Using Pressure Gradient Vectors. Earl T. Riddiough, July 1972. (COM 72 11146)
79 Climate of Stockton, California. Robert C. Nelson, July 1972. (COM 72 10920)
80 Estimation of Number of Days Above or Below Selected Temperatures. Clarence M. , October 1972. (COM 72 10021)
81 An Aid for Forecasting Summer Maximum Temperatures at Seattle, Washington. Edgar G. Johnson, November 1972. (COM 73 10150)
82 Flash Flood Forecasting and Warning Program in the Western Region. Philip Williams, Jr., Chester L. Glenn, and Roland L. Raetz, December 1972, (Revised March 1978). (COM 73 10251)
83 A comparison of Manual and Semiautomatic Methods of Digitizing Analog Wind Records. Glenn E. Rasch, March 1973. (COM 73 10669)
86 Conditional Probabilities for Sequences of Wet Days at Phoenix, Arizona. Paul C. Kangieser, June 1973. (COM 73 11264)
87 A Refinement of the Use of K-Values in Forecasting Thunderstorms in Washington and Oregon. Robert Y.G. Lee, June 1973. (COM 73 11276)
89 Objective Forecast Precipitation Over the Western Region of the United States. Julia N. Paegle and Larry P. Kierulff, September 1973. (COM 73 11946/3AS)
91 Arizona "Eddy" Tornadoes. Robert S. Ingram, October 1973. (COM 73 10465)
92 Smoke Management in the Willamette Valley. Earl M. Bates, May 1974. (COM 74 11277/AS)
93 An Operational Evaluation of 500-mb Type Regression Equations. Alexander E. MacDonald, June 1974. (COM 74 11407/AS)
94 Conditional Probability of Visibility Less than One-Half Mile in Radiation Fog at Fresno, California. John D. Thomas, August 1974. (COM 74 11555/AS)
95 Climate of Flagstaff, Arizona. Paul W. Sorenson, and updated by Reginald W. Preston, January 1987. (PB87 143160/AS)
96 Map type Precipitation Probabilities for the Western Region. Glenn E. Rasch and Alexander E. MacDonald, February 1975. (COM 75 10428/AS)
97 Eastern Pacific Cut-Off Low of April 21-28, 1974. William J. Alder and George R. Miller, January 1976. (PB 250 711/AS)
98 Study on a Significant Precipitation Episode in Western United States. Ira S. Brenner, April 1976. (COM 75 10719/AS)
99 A Study of Flash Flood Susceptibility-A Basin in Southern Arizona. Gerald Williams, August 1975. (COM 75 11360/AS).
102 A Set of Rules for Forecasting Temperatures in Napa and Sonoma Counties. Wesley L. Tuft, October 1975. (PB 246 902/AS)
103 Application of the National Weather Service Flash-Flood Program in the Western Region. Gerald Williams, January 1976. (PB 253 053/AS)
104 Objective Aids for Forecasting Minimum Temperatures at Reno, Nevada, During the Summer Months. Christopher D. Hill, January 1976. (PB 252 866/AS)
105 Forecasting the Mono Wind. Charles P. Ruscha, Jr., February 1976. (PB 254 650)
106 Use of MOS Forecast Parameters in Temperature Forecasting. John C. Plankinton, Jr., March 1976. (PB 254 649)
107 Map Types as Aids in Using MOS PoPs in Western United States. Ira S. Brenner, August 1976. (PB 259 594)
108 Other Kinds of Wind Shear. Christopher D. Hill, August 1976. (PB 260 437/AS)
109 Forecasting North Winds in the Upper Sacramento Valley and Adjoining Forests. Christopher E. Fontana, September 1976. (PB 273 677/AS)
110 Cool Inflow as a Weakening Influence on Eastern Pacific Tropical Cyclones. William , November 1976. (PB 264 655/AS)
112 The MAN/MOS Program. Alexander E. MacDonald, February 1977. (PB 265 941/AS)
113 Winter Season Minimum Temperature Formula for Bakersfield, California, Using Multiple Regression. Michael J. Oard, February 1977. (PB 273 694/AS)
114 Tropical Cyclone Kathleen. James R. Fors, February 1977. (PB 273 676/AS)
116 A Study of Wind Gusts on Lake Mead. Bradley Colman, April 1977. (PB 268 847)
117 The Relative Frequency of Cumulonimbus Clouds at the Nevada Test Site as a Function of K-Value. R.F. Quiring, April 1977. (PB 272 831)
118 Moisture Distribution Modification by Upward Vertical Motion. Ira S. Brenner, April 1977. (PB 268 740)
119 Relative Frequency of Occurrence of Warm Season Echo Activity as a Function of Stability Indices Computed from the Yucca Flat, Nevada, Rawinsonde. Darryl Randerson, June 1977. (PB 271 290/AS)
121 Climatological Prediction of Cumulonimbus Clouds in the Vicinity of the Yucca Flat Weather Station. R.F. Quiring, June 1977. (PB 271 704/AS)
122 A Method for Transforming Temperature Distribution to Normality. Morris S. Webb, Jr., June 1977. (PB 271 742/AS)
124 Statistical Guidance for Prediction of Eastern North Pacific Tropical Cyclone Motion - Part I. Charles J. Neumann and Preston W. Leftwich, August 1977. (PB 272 661)
125 Statistical Guidance on the Prediction of Eastern North Pacific Tropical Cyclone Motion - Part II. Preston W. Leftwich and Charles J. Neumann, August 1977. (PB 273 155/AS)
126 Climate of San Francisco. E. Jan Null, February 1978. (Revised by George T. Pericht, April 1988 and January 1995). (PB88 208624/AS)
127 Development of a Probability Equation for Winter-Type Precipitation Patterns in Great Falls, Montana. Kenneth B Mielke, February 1978. (PB 281 387/AS)
128 Hand Calculator Program to Compute Parcel Thermal Dynamics. Dan Gudgel, April 1978. (PB 283 080/AS)
129 Fire whirls. David W. Goens, May 1978. (PB 283 866/AS)
130 Flash-Flood Procedure. Ralph C. Hatch and Gerald Williams, May 1978. (PB 286 014/AS)
131 Automated Fire-Weather Forecasts. Mark A. Mollner and David E. Olsen, September 1978. (PB 289 916/AS)
132 Estimates of the Effects of Terrain Blocking on the Los Angeles WSR-74C Weather Radar. R.G. Pappas, R.Y. Lee, B.W. Finke, October 1978. (PB 289767/AS)
133 Spectral Techniques in Ocean Wave Forecasting. John A. Jannuzzi, October 1978. (PB291317/AS)
134 Solar Radiation. John A. Jannuzzi, November 1978. (PB291195/AS)
135 Application of a Spectrum Analyzer in Forecasting Ocean Swell in Southern California Coastal Waters. Lawrence P. Kierulff, January 1979. (PB292716/AS)
136 Basic Hydrologic Principles. Thomas L. Dietrich, January 1979. (PB292247/AS)
137 LFM 24-Hour Prediction of Eastern Pacific Cyclones Refined by Satellite Images. John R. Zimmerman and Charles P. Ruscha, Jr., January 1979. (PB294324/AS)
138 A Simple Analysis/Diagnosis System for Real Time Evaluation of Vertical Motion. Scott H and James R. Fors, February 1979. (PB294216/AS)
139 Aids for Forecasting Minimum Temperature in the Wenatchee Frost District. Robert S. , April 1979. (PB298339/AS)
140 Influence of Cloudiness on Summertime Temperatures in the Eastern Washington Fire Weather district. James Holcomb, April 1979. (PB298674/AS)
141 Comparison of LFM and MFM Precipitation Guidance for Nevada During Doreen. Christopher Hill April 1979. (PB298613/AS)
142 The Usefulness of Data from Mountaintop Fire Lookout Stations in Determining Atmospheric Stability. Jonathan W. Corey, April 1979. (PB298899/AS)
143 The Depth of the Marine Layer at San Diego as Related to Subsequent Cool Season Precipitation Episodes in Arizona. Ira S. Brenner, May 1979. (PB298817/AS)

NOAA TECHNICAL MEMORANDUM
NWS WR-246

A WESTERN REGION GUIDE TO THE ETA-29 MODEL

Mike Staudenmaier, Jr.
WRH-SSD/NWSFO SLC
Salt Lake City, UT

March 1997

UNITED STATES
DEPARTMENT OF COMMERCE
William M. Daley, Secretary

National Oceanic and
Atmospheric Administration
D. James Baker, Under
Secretary and Administrator

National Weather Service
Elbert W. Friday, Jr., Assistant
Administrator for Weather Services

This publication has been reviewed
and is approved for publication by
Scientific Services Division,
Western Region

Delain A. Edman, Chief
Scientific Services Division
Salt Lake City, Utah

Foreword

This report is a compilation of a series of Technical Attachments that the author has written during 1996, referencing and documenting different aspects of the Eta-29 model (commonly referred to as the Meso Eta model). It is hoped that this information is complete enough so that readers may understand the strengths and weaknesses of the model, through knowledge of how the parameterizations, initialization, and integration of the model operate. This should allow forecasters to interpret the model guidance produced by the Eta-29 in a more scientific light.

I would like to acknowledge all the good folks at NCEP who have been invaluable in my quest for the answers regarding the model, and to Western Region SSD for allowing me the opportunity to write about this model, which is proving to be a superior source for numerical weather prediction guidance. Special thanks go to Michael Baldwin, Geoffrey DiMego, Thomas Black, Jon Mittelstadt, and Andy Edman for providing encouragement and assistance in the publication of these Technical Attachments, and ultimately of this Technical Attachment.

TABLE OF CONTENTS

TABLE OF FIGURES

A WESTERN REGION GUIDE TO THE ETA-29 MODEL

Mike Staudenmaier, Jr.
WRH-SSD/NWSFO SLC
Salt Lake City, UT

I. INTRODUCTION

The National Center for Environmental Prediction (NCEP), formally known as NMC, has been developing and running numerical weather prediction models operationally since 1955. The first operational model was an equivalent-barotropic model and from this model came the barotropic mesh model, which remained in use through 1985. The next major change to models came with the introduction of a six-layer hemispheric primitive equation (PE) model in 1966. A limited-area version of this model, known as the Limited-area Fine-mesh Model (LFM), became operational in 1971. It was replaced in 1977 by a finer-mesh model, known as the LFM II, but in 1981 the original grid mesh was restored. In August 1980, the current seven-layer PE model was replaced by a twelve-layer global spectral model, which has evolved considerably since then into the Medium-Range Forecast model (MRF) and the Aviation (AVN) model. In the spring of 1985, a new Regional Analysis and Forecast System (RAFS) was introduced with the Nested Grid Model (NGM) serving as the forecast model. In June 1993, the Eta model replaced the LFM as the 'early' model run with 80 km resolution and 38 vertical layers. In early 1996, a 29 km version of the Eta model was tested in the field, with very positive results. By August 1996, the Eta-29 (commonly referred to as the Meso Eta model) was fully operational and proving its worth to the field.

II. BASIC DESCRIPTION OF THE MODEL

As of this writing, the Eta-29 has a horizontal grid spacing of approximately 29 km and 50 vertical levels, with layer depths that range from 20 m in the planetary boundary layer to 2 km at 50 mb (Fig. 1). The eta coordinate, defined by Mesinger (1984), was used in order to remove the large errors which are known to occur when computing the horizontal pressure gradient force, as well as the advection and horizontal diffusion, along a steeply sloped coordinate surface. This coordinate system makes the eta surfaces quasi-horizontal everywhere as opposed to sigma surfaces which can be steeply sloped. Thus, this model should perform well in areas with widely varying topography. Because the eta coordinate is pressure based and normalized, it leads to a much simpler solution of the equations of motion in areas such as the pressure gradient force, horizontal advection, and diffusion. The eta coordinate is defined by the relationship:

$$\eta = \left(\frac{p - p_T}{p_{sfc} - p_T}\right)\left[\frac{p_{ref}(z_{sfc}) - p_T}{p_{ref}(0) - p_T}\right]$$

where T refers to the top of the domain (25 hPa), sfc is at the models lower boundary, and ref is a reference pressure state that is a function of distance above sea level. Additional information in regards to the eta coordinate can be found in Black (1994).

The semi-staggered Arakawa E grid (Arakawa and Lamb 1977) is the basis of the model's horizontal structure. A sample subset of the E grid can be seen in Fig. 2. Each H represents a "mass" variable point (such as temperature or moisture) and each V represents both horizontal components of the wind. The distance "d" is the spacing between adjacent H or adjacent V points, and the magnitude of this distance is commonly used to indicate the model's horizontal resolution. The E grid lies upon a rotated latitude-longitude framework. This coordinate system is created by simply rotating the earth's entire geographic latitude-longitude grid so as to place the intersection of the equator and the prime meridian over the center of the forecast area. In doing this, the convergence of the meridians is minimized over the forecast area. Each grid box thus consists of a mass point surrounded by four velocity points, all of which lie along parallels and meridians of rotated latitude-longitude.

The model topography is represented as discrete steps whose tops coincide exactly with model layer interfaces. In determining their elevations, each 29 km horizontal grid box is first divided into 16 subboxes. Mean elevations for each of these 16 subboxes are calculated from archived topography data. Using these values, the maximum mean value from each of the four rows and four columns are determined, resulting in eight intermediate terrain values. The mean of these eight values are taken to yield an intermediate value for the step height. Having already determined the height of each model layer interface based on the standard atmosphere and the specified distribution of vertical resolution, the final step elevation is found by moving the mean either up or down to the closest layer interface in the model domain.

A schematic vertical cross section through the lowest layers of the domain (Fig. 3) illustrates the various aspects of the horizontal and vertical structures in the model. Within each model layer, T represents "mass" variables such as temperature and moisture, while U represents both horizontal components of the wind; p_s is the surface pressure.

All velocity points that lie on the edge of a step are given the value of zero and retain it throughout the forecast (these are indicated by the circled U's in Fig. 3). This is called the no-slip condition. Because of this condition, if any grid point in the model lies in a "hole", where it is surrounded by steps of greater elevation, all four surrounding velocity points would be zero. If this is the case, this "hole" is raised to the point where at least one of the surrounding velocities is nonzero. This is necessary to ensure that all grid boxes that are above the model surface have some horizontal divergence to produce vertical advections.

The assimilation procedure begins 3 hours prior to the actual start of the forecast. At t-3 hours, or at 0000 UTC and 1200 UTC, a first guess is provided by the Global Data Assimilation System (GDAS) and applied to the Eta-29 coordinate system. The model then integrates for 3 hours which provides the first guess to the new "initial" analyses at 0300 UTC and 1500 UTC which utilizes all new available data, comprised of numerous aircraft reports, NEXRAD, profiler, and satellite observations. Finally, the 33 hour forecast is run.

The model's boundary data on its single outermost row of points are obtained by direct interpolation from the aviation run of the global spectral Medium-Range Model (MRF). At inflow boundary points, all of the prognostic variables are determined by the MRF data, while at outflow points, the velocity components tangential to the boundary are extrapolated from the interior of the integration domain. The values of the second outermost row are a blend of those along the boundary and those in the third row which are part of the true integration domain.

PROGNOSTIC VARIABLES

The primary prognostic variables in the Eta-29 model are temperature, specific humidity, horizontal wind components, surface pressure, cloud water/ice and turbulent kinetic energy. The split-explicit approach is used in producing forecasts based on these quantities. This means that during each time step, after each process is computed, each of the primary variables is updated and the integration continues. The time step in the Eta-29 model is about 72 seconds.

PARAMETERIZATION SCHEMES

Both grid scale and convective precipitation in the model are predicted quantities. After every two adjustment time steps, or about every 2.5 minutes, grid-scale precipitation is formed if certain criteria are met, determined mainly by the amount of cloud water/ice as a function of temperature and vertical level in the model. Part or all of this precipitation may evaporate as it falls to the model surface if it falls though layers where the relative humidity is less than a predetermined value. Convective precipitation, based on the Betts-Miller cumulus parameterization (Betts 1986; Betts and Miller 1986) with some modifications based on work by Janjic' (1994), is computed every four adjustment time steps, or about every five minutes. Non-precipitating shallow convection serves to carry moisture upward and maintain low-level temperature inversions. Deep convection transports heat and moisture upward and produces rainfall. For both types of convection, reference profiles of temperature and specific humidity are constructed using the values of these variables that are present in the model in conjunction with specified vertical gradients that were determined from numerous observations in the field. The model values are then relaxed toward these reference profiles. The rainfall is deduced from the net negative change of specific humidity in the model's deep convective cloud; if the net change in water vapor is positive (i.e. net evaporation occurred rather than

condensation), no adjustment of the variables is made at that grid point. An explicit cloud water prediction scheme (Zhao et al. 1991) is also incorporated in the model and determines the cloud water/ice ratio used in the precipitation process mentioned above.

In this explicit cloud water prediction scheme, the mixing ratio of cloud water and ice is an additional prognostic variable. This explicit cloud water prediction scheme takes into account the physical processes of evaporation, condensation, melting, freezing, sublimation, and deposition which occur in the atmosphere. The amount of condensed cloud water is predicted throughout the domain and a three dimensional array indicates whether that condensate is liquid or solid. The cloud phase is strictly a function of temperature: (I) if T<0 °C then the cloud is liquid; (ii) if T<-15 °C then the cloud is ice; (iii) for intermediate temperatures, the cloud will be ice only if cloud ice existed in the same grid box or any box directly above during the previous time step. Thus, ice is not allowed to develop in the cloud process until the temperature reaches -15 °C. Cloud water is allowed to evaporate or sublimate when the relative humidity drops below a critical value which differs for locations in the model which are located above water or above land. The model does not allow for more than one phase of cloud water within any given grid box, although the grid-scale precipitation within a box can be both liquid and solid. Currently, this scheme is not linked to the convective parameterization.

The current version of the radiation package used in the model is based on the model developed at the Geophysical Fluid Dynamics Laboratory. It used to require the specification of only three levels of cloud (low, middle, and high), which were determined from the cloud amounts in all of the model layers. These were calculated by a simple relation based solely on the relative humidity. Now, however, the explicit cloud model is used to derive moisture and cloud at all model layers, leading to a much more realistic result.

The soil package which was developed for the Eta-29 provides a more rigorous description of the ground processes than those available in other operational numerical models. This soil model now employs two predictive soil layers. The upper layer is 10 cm thick and the lower layer is 190 cm thick. The prognostic temperature for these layers is valid at their centers. Internal vertical heat and moisture fluxes are computed. The initial soil temperature and moisture are taken from the 6-hour forecast from the Global Data Assimilation System. Soil type, vegetation type, and green vegetation fraction are specified as functions of geographic location and the latter also as a function of time. Variability in these quantities permits a much improved handling of such factors as ground permeability, transpiration effects, and albedo. Heat exchange with the atmosphere takes place either at the bare ground interface or on the plant canopy composite. Moisture exchange occurs with the bare soil and with condensed water on plant surfaces as well as though transpiration via leaf pores.

The vertical turbulent exchange follows that described by Mellor and Yamada (1974, 1982) and is carried out every eight advective time steps. Exchange between model layers in the free atmosphere is based on the Mellor-Yamada Level 2.5 Model. In this scheme, turbulent kinetic energy is a fully prognostic variable that is carried on layer interfaces in the Eta-29. The predicted turbulent kinetic energy is then used to compute the exchange coefficients for the transfer of heat, moisture, and momentum between adjacent model layers. The exchange coefficients are used to modify the prognostic variables in the grid box though which the transfer is occurring. Surface fluxes of moisture and heat between the model surface and the first model layer are computed using Monin-Obukov functions (Lobocki,1993).

The next section of this paper will discuss the initialization procedure in the Eta-29 model along with potential problems with this procedure for the Western Region.

III. THE INITIALIZATION PROCEDURE

The initialization procedure for the Eta-29 begins three hours prior to the actual start of the forecast model run. At t-3 hours, or at 0000 UTC, 0600 UTC, 1200 UTC, and at 1800 UTC, a first guess is provided by the Global Assimilation System (GDAS) using all available data. This first guess is applied to the Eta-29 coordinate system. The original analysis is converted from spectral space (off of the AVN model grid) to the Eta model native grid and interpolated vertically to eta coordinate surfaces. This adjusted "first guess" is then interpolated to each observation location and the observed increments (observed - first guess) are computed. A multi-variate Optimum Interpolation (OI) analysis of the observed increments is performed on the Eta-29 model grid and is used to modify and update the "first guess". The only variables in the model which are updated during the OI analysis are temperature (T), the u- and v-components of the wind field (u,v), the specific humidity (q), and the pressure at the model terrain level (p^*). The model then integrates for three hours, at which time another OI analysis is performed on all observed data which has been received over the past 1.5 hours that is in the form just mentioned (T,u,v,q,p^*). The grids are modified based on these observed increments from the OI analysis and these new grids provide the initial analyses for the 0300 UTC and 1500 UTC runs of the model.

These new analyses benefit from a later cutoff time for data injestion, utilizing new data during the last 1.5 hours of the initialization period. This additional data is comprised of numerous aircraft reports, surface observations, profilers, and limited satellite observations. Once all of this data has been assimilated into the initial analysis, the 33-hour forecast is run. Boundary conditions for both the assimilation and model forecast are obtained directly from the AVN run of the NMC Global Spectral Model, thus one could consider the Eta-29 to be a nest inside the AVN model run.

DISCUSSION OF PRESENT PROBLEMS

Due to resolution differences between the model and reality, there are still locations that will likely not see the full potential of this assimilation process. Many places in the Western Region fall into this category. Even at 29 km resolution, many of the sharp gradients in topography, especially narrow valleys or mountain ranges, are not represented in the model topography. Numerous cities in the Western Region are located in these types of locations. Thus, there are many observing stations in the Western Region which actually lie below the model surface. *Any data which in reality is greater than 25 mb below the model surface is not used in the assimilation process.* Additionally, many second and third order surface observation points (103 of them in the Western Region) do not report station pressure at the station elevation. These sites must be thrown out since the assimilation scheme does not know at what level to place the data. Because of these facts, only 14% (20/144) of the NWS surface observation network in the Western Region will generally make it into the initialization of the Eta-29. In the Western Region, the locations most likely to have their surface data used in the Eta-29 model are much of Washington, portions of southern and central California, northeastern Arizona, western Idaho, and portions of central Montana (Fig. 4). Currently, no surface information from Nevada or Utah makes it into the Eta-29 model.

A brief explanation of how surface data is processed during the assimilation procedure is needed at this point. As mentioned above, only T, u, v, q, and p* are used in the assimilation process. Additionally, because of how the models are set up for integration between levels, these variables exist at the mid-point of the layers, not at the layer interfaces (at the bottom or top of the layer). *Thus, in reality, there is no model surface.* Nor is there a level at 2 meters, or at 10 meters. These values are derived from the values at the mid-point of the lowest layer in the model domain above the model terrain. Because of this, the first place in the model where information is needed to correct the first-guess towards reality is actually at the mid-point of the first layer above the model's terrain, which over elevated terrain can be a substantial distance above the model terrain and therefore even further away from reality where the actual observation was taken. In order to generate the corrections needed to the first guess when the observation is below the lowest data level in the model requires extrapolation 'underground' through the model surface and upward into the model's atmospheric portion of the profile. This is a very risky proposition for which no real effective, or realistic, procedure exists. Thus, to make the assimilation procedure easier, this extrapolation is limited to no more than 25 mb. So if a piece of observed data requires extrapolation of more than 25 mb to reach the mid-point of the first model layer, it doesn't get used. This is the current method used in both the NGM and the ETA models since the development of the NGM model in 1983. The global model does not allow any extrapolation of data below the first sigma layer mid-point, so even more surface data in the Western Region is thrown out in that model.

Additionally, data cutoff occurs in radiosonde data as well because of this effect. In the model assimilation process, the model will use any data from a radiosonde which is above the mid-point of the lowest model layer and throw out any data which is located below this level, even if the model surface is located well above the real surface. Since the free atmosphere is being used as the new 'surface', low-level surface moisture gradients may be weakened or destroyed, and many times this will create a drier and cooler surface than what actually exists in reality. Any low-level temperature gradients may also be weakened by this process as well as destroying low-level radiative inversions and frontal structure. The most susceptible locations for this loss of near-surface data appears to be in a belt from Medford, OR to Grand Junction, CO, covering much of the Great Basin region. Figure 5 is a map showing the most likely areas for data loss in radiosondes. Figure 6 shows typical depths of data loss for many of the radiosondes in the western portion of the United States. As can be seen, the Eta-29 improves over the Eta model on the data loss problem in most places, however, at some sites it has become slightly worse. Some sites, like Salt Lake City (SLC) are still losing the lowest 65 mb of the raob during the assimilation process. Clearly though, the benefits outweigh the drawbacks.

Why is the Great Basin so prone to data loss during the initialization process? A likely reason may have to do with the way model topography is derived. In determining the surface elevation for a particular area, each 29 km horizontal grid box is first divided into 16 subboxes. Mean elevations for each of these 16 subboxes are calculated from official United States Geological Survey (USGS) topographical data. Using these values, the maximum mean value from each of the four rows and four columns are taken to yield an intermediate value for the grid box surface elevation. The mean of these eight values are taken to yield an intermediate value for the model grid box. The final grid elevation is found by moving this mean value up or down to match the closest vertical layer in the model domain. Due to the particular nature of topography in the Great Basin, with numerous narrow north-south oriented mountain ranges with broad valleys, the model topography would be biased toward the higher elevation of the narrow mountains. Almost all of the surface data in the Great Basin however, comes from locations on the valley floors. This likely leads to most surface observation points being located more than 25 mb below the model topography and thus, being thrown out during the assimilation process.

Currently, no mesoscale information is implemented in the initialization process. Even if mesoscale data sources become available in the Western Region for model ingestion, it is still questionable if much of this data would even pass the assimilation process, or if most of it would be thrown out, especially when referring to mesonets of surface observations occurring in areas previously mentioned. Additionally, only temperature, specific humidity, and station pressure are being ingested from those surface observations which make it into the assimilation process. *No observed surface wind data*

is currently being used in the model, nor in any of the NCEP suite.

At this time, the cloud model (Zhao et al., 1996) in the Eta-29 model is not initialized with cloud water or ice. Thus, the model must 'spin-up' or create cloud water/ice during the first few hours. This creates a slight lag in the development of precipitation as the cloud model must reach saturation before any precipitation can occur. Additionally, once the cloud model saturates, model clouds may develop in different locations than reality, as model clouds must develop due to model physics, without any basis on their actual location in reality.

The soil model in the Eta-29 is currently not initialized with real-time moisture or temperature values, but rather with climatological values. Currently there is no real-time accessible nationwide network of root-zone soil moisture or temperature observations available for assimilation. This poor initialization of soil moisture and temperatures can cause problems in the development of precipitation in the model. One reason is that soil moisture and temperature gradients can occasionally act as focusing mechanisms for the initiation and sustenance of convection. Additionally, evaporation of soil moisture into the free atmosphere can enhance low-level moisture in the atmosphere, leading to heavier rainfall potential and possible convection. Vegetation type and soil type in the model are based on 1 degree by 1 degree fixed climatological values. The green vegetative fraction, however, is based on 0.15 degree by 0.15 degree monthly fields based on a 5 year climatology. These monthly fields of green vegetative fraction are interpolated to actual days of the year, so the values can change slightly from day to day. Additional resolution of these fields is necessary at 29 km resolution, and will be even more necessary at 10 km resolution.

The radiation scheme in the model uses climatological values of carbon dioxide and ozone concentrations, which are not allowed to evolve during the forecast integration. Surface albedo is derived from 1 degree by 1 degree quarterly climatological fields which are then interpolated to actual days of the year. This first guess of albedo is then allowed to evolve based on snow cover and snow depth, green vegetation fraction, sea ice, and model clouds, among other things. In a mesoscale model with a short forecast period, it might not be that important to have actual values of the chemical composition of the atmosphere. However, having values of actual surface albedo for initialization might improve the radiation scheme slightly. Satellite data is not used in the initialization of the radiation model, and since there is no cloud water/ice in the cloud model, the radiation package does not reflect reality in terms of cloud cover.

Satellite data is currently used only to nudge the current analysis towards reality. With the OI analysis, satellite observations must be in the form of temperature, wind, specific humidity, or pressure at the model surface to be used. Almost all satellite data is not in this form, and thus cannot be used currently. In the current analysis scheme, the usefulness of satellite data only includes GOES cloud drift winds, TOVS deep-layer thicknesses over the oceans, and SSMI

total column precipitable water. The cloud drift winds are used to augment upper air data and to add some detail to the upper atmospheric structure. Over the ocean, moisture profiles are subjectively determined based on certain cloud signatures and then added to the OI scheme. This data is low resolution (around 200 km resolution with 6 levels of relative humidity data) and can only be determined when certain cloud signatures exist over the ocean. SSMI precipitable water products are also being used in the assimilation process. This data has good horizontal resolution, but has NO information on how that moisture is distributed through the vertical column. Thus, this moisture can only be used to do an adjustment of the model precipitable water guess field. As stated above, no information from the satellite data is used in conjunction with the cloud model or the radiation package. Currently, the retrieved single layer temperatures and satellite-derived vertical profiles of temperature and moisture are not accurate enough to use in the OI analysis.

Even with all these problems in the way data is assimilated into the model, the Eta-29 still manages to capture much of the details of the day-to-day weather pattern. Due to its 29 km resolution, the Eta-29 likely manages to assimilate more data than any of the other models in the current NCEP operational numerical model suite, leading to better forecasts. Future plans to improve on the assimilation procedure can be found in section 9. The next section will discuss the convective parameterization scheme in the model along with current strengths and weaknesses in the Western Region.

IV. THE CONVECTIVE PARAMETERIZATION SCHEME

THE BASIS OF THE SCHEME

The Eta-29 model employs a convective parameterization scheme developed by Betts and Miller (1986) and further refined by Janjic' (1994) (hereafter BMJ scheme). The primary objective of the parameterization scheme is to ensure that the local vertical temperature and moisture structures, which in nature are strongly constrained by convection, be realistic in the model (Betts 1986). Since convective regions have characteristic temperature and moisture structures which can be observed, they were used as a basis for a convective adjustment procedure. In the BMJ scheme, the temperature and moisture profiles at a given grid point are relaxed simultaneously toward a profile type which has been observed in nature. The model first checks for deep convection, and then for shallow convection. By relaxing the profiles at a grid point simultaneously, the model always maintains a realistic vertical temperature and moisture structure in the presence of convection. By doing this simple adjustment, it is believed that the subgrid-scale cloud and mesoscale processes which created these structures will be adequately represented. The BMJ scheme will be discussed in terms of the shallow convective and then the deep convective parameterizations.

SHALLOW CONVECTIVE SCHEME

Cumulus convection is a moist mixing process between the subcloud layer and

drier air aloft, and not surprisingly, the thermodynamic structure tends towards a mixing line (Betts, 1986). Betts (1982) has defined the mixing line as a linear approximation between the two source regions, i.e. the subcloud layer and the drier air aloft. To determine the mixing line, saturation points are used. These saturation points are simply the locations where the parcels become saturated after lifting. The BMJ shallow convective parameterization uses this mixing line approach to create modified soundings reflecting the moist mixing process.

In the BMJ shallow convective parameterization, the most unstable parcel at each grid point is found, and the model calculates its lifted condensation level (LCL), which becomes the cloud base. This parcel is lifted to calculate the cloud top, which is simply determined as the last model level where the lifted parcel is warmer than the surrounding environment, i.e. at or just below the equilibrium level (EL). Additionally, the cloud top is forced to be below 450 mb, so that the shallow convective scheme doesn't modify the upper troposphere. The model then determines if the "cloud" is a) greater than 10 mb deep, b) less than 290 mb deep, and c) at least 2 model layers deep. If these criteria are satisfied at a grid point, a line connecting the saturation point of the cloud base with the saturation point of the cloud top is determined. This line is called the mixing line. If any of these criteria are not met, the grid point is skipped.

At this point, the model determines the modifications needed for the temperature profile. This is done simply by connecting the temperature at the model level just below cloud base up to the model level just above cloud top, keeping the slope of this line the same slope as that of the mixing line (Fig. 7). The profile is then connected to the remainder of the sounding below cloud base and above cloud top with no modifications applied anywhere else. At this point, the newly modified temperature profile is then corrected so that the net latent heat release is zero, which means that you end up with no precipitation produced by this process.

Next, the model determines which modifications are needed to create the moisture profile. This process is somewhat complicated, but basically the modified moisture profile is modified so that the following two constraints will be met:

1) No precipitation will reach the ground, i.e. the net latent heat release due to the moisture change is zero, or the total water vapor in the cloud is unchanged.

2) The total entropy change due to the shallow convective parameterization must be a small positive quantity. The entropy change due to the temperature change must be negative (since the temperatures cooled), therefore the entropy change due to the moisture change must be positive. In the model, the total entropy change is set to be 5% larger than the magnitude of the entropy change due to the change in temperature.

What this means, is that the moisture will be moved upwards, so that net drying will occur near the cloud base, and net moistening will occur near the cloud top. It mimics the process of condensation

near cloud base, where there is latent heat release (warming) and water vapor changes state to liquid (drying of water vapor). Conversely, it mimics evaporation near the cloud top, where there is cooling and moistening occurring with respect to water vapor. The adjustments occur in a way so that the net change to the sounding results in no precipitation produced. The model takes about 40 minutes to gradually apply these modifications to better simulate the convective process.

DEEP CONVECTIVE SCHEME

The BMJ deep convective parameterization scheme is based on the observation that deep convection is a thermodynamically driven process that transports heat and moisture upward in order to remove or reduce conditional instabilities (Janjic 1994). Precipitation is usually produced during this process. The vertical transportation of heat and moisture is accomplished through the process of mixing, as with the shallow convection.

In the BMJ deep convective parameterization, the model first searches all the parcels within the lowest 130 mb of the model surface and finds the most unstable parcel at each grid point. Just like in the shallow convective parameterization, the model calculates the LCL of this most unstable parcel and calls the model layer below this point, the cloud base. The cloud base must be at least one layer above the lowest model layer and/or at least 25 mb above the middle of the lowest layer. If the cloud base does not satisfy these requirements, the cloud base is lifted accordingly. The parcel is then lifted to calculate the cloud top, which again is simply the model layer below or at the EL. If the depth of the cloud is greater than 290 mb, the deep convective parameterization will continue, otherwise this point will be checked to see if the shallow convective parameterization needs to be applied.

If the cloud is greater than 290 mb in depth, the model will then determine the modifications needed for the temperature profile. From the cloud base to the ambient (environmental) freezing level, the temperature profile is modified to be 90% of the slope of the moist adiabat which goes through the cloud base (Fig. 8). Betts (1982) found that the slope of the temperature profile in deep convection approached this slope as opposed to the slope of the moist adiabat. This suggested that the atmosphere remains slightly unstable, so that air rising in vigorous cumulus towers remains buoyant until its cloud water is converted to precipitation-size particles. From the ambient freezing level to the cloud top, a straight line is drawn to connect the points.

Next, the model determines which modifications are needed to create the moisture profile. To understand how the modified moisture profile is created, we need to define a term called saturation pressure deficit (DSP). Betts (1982) defined the saturation pressure deficit as the difference between the air parcel saturation level and the pressure level of that air parcel. Therefore, it is the distance (in Pa) that a parcel needs to be lifted to reach saturation.

It is at this point that the parameterization becomes somewhat more difficult to understand. A parameter is calculated called the "cloud efficiency" (Janjic 1994). This parameter measures the ability of the convective column to transport the enthalpy upward and at the same time produce as little precipitation as possible. At this point, an assumption is made that the convective forcing is proportional to an increasing function of the cloud efficiency. In this way, heavy precipitation which normally would just continue to develop and fall, could be modified in the case of low cloud efficiency. This was done in order to decrease the amount of spurious heavy rain bulls eyes which occurred occasionally over warm water, where there was an abundant source of low level moisture and instability, with no way to turn the precipitation off once it started.

Two extremes of cloud efficiency were determined for the deep convection parameterization: 1) a cloud that is in a predominantly mixing stage with high cloud efficiency and not much rainfall, and 2) a cloud that is in a predominantly rain producing stage with low cloud efficiency. DSP's are assigned for these two extremes, so that any cloud efficiency will fit between them. The DSP values will also be slightly lower over water. Three anchor points in the cloud are assigned specific DSP's: 1) cloud base, 2) cloud top, and 3) the ambient freezing level. Typically over land, the DSP at cloud base is around -48 mb, the DSP at the ambient freezing level is around -70 mb, and the DSP at the cloud top is around -22 mb. All of the DSP's for all of the other layers in between are linearly interpolated between these anchor points. Since the DSP at the freezing level has the biggest magnitude, it will be the driest point of the moisture profile, which agrees with the findings of Betts (1986) of a theta-e minimum very near the freezing level. Given a temperature and a DSP profile, it becomes trivial to calculate the specific humidity, and the modified moisture profile.

Again, corrections need to be made to the profiles in order to conserve enthalpy. By doing this, we are saying that if it does rain, the net latent heat release will be in balance with the net moisture change due to condensation. Precipitation is directly calculated from the amount of latent heat produced by the modification of the soundings. If the precipitation is not positive, or if the entropy of the grid point decreases, the deep convection parameterization is aborted, and the shallow convective parameterization is used at that point. *Thus, the way to get precipitation out of the deep convective scheme is to have the modified moisture profile become drier and the modified temperature profile become warmer.* This means that the adjustment created warming and drying such that the net enthalpy is unchanged, but allowed for latent heat (via condensation) to be released and precipitation to fall out of the cloud. As with the shallow convective parameterization, these modifications to the airmass take about 40 minutes to occur to better simulate nature.

THE BMJ CONVECTIVE SCHEME IN THE WEST

Results with precipitation output from the Eta-29 model have been fairly positive

with many case studies showing the improvement of the model resolution on the placement and amount of predicted precipitation (Burks and Staudenmaier 1996; Gartner, Baldwin, and Junker 1996; Schneider et al., 1996). However, verification of convective precipitation in the Western Region has been less impressive with serious deficiencies in the production of convective precipitation in areas of topography (Baldwin and Black 1996; Swanson 1995). Figure 9 is an example of a typical pattern of convective precipitation, indicating how convective precipitation appears to be limited to locations below 4000 feet in elevation. The remainder of this section will investigate some of the potential strengths and weaknesses in the BMJ convective scheme.

The main strength of the BMJ scheme is that it couples simplicity with adequate skill in developing convection. Since numerical models are constrained to discrete time steps and resolutions, it is necessary to parameterize any physical process which occurs on a scale smaller than that resolvable by the model. The BMJ convective parameterization is purely a convective adjustment scheme. This means that once the parameterization is initiated, the atmosphere is adjusted towards a post-convective environment, with precipitation possibly developing. Convective adjustment is a simple and economical method (in terms of computer resources) of parameterizing convection. However, since it bypasses most of the physical processes involved, it has limited flexibility and will likely have increasing limitations as model resolution continues to improve.

Since, convection is not explicitly created in the model, mesoscale features such as updrafts, downdrafts and associated momentum transfer to the surface are not accommodated. No changes are made to the wind shear profile or to the subcloud layer. This scheme is not linked in any way to the explicit cloud prediction scheme of the model, except through modification of the model relative humidity fields. Because of these limitations, convection in the model will likely not look realistic in terms of propagation or additional development due to outflow boundaries.

Because the BMJ scheme relies solely on instability for the generation of convection, this scheme should perform better than the Kuo scheme, which is currently used in the NGM model, in situations where daytime heating is the major contributor to convective initiation. This is because the Kuo scheme also relies on low-level convergence for convective initiation, which may not occur with the course resolution of the model. This also leads to the probability that the BMJ scheme will allow for a faster "spin-up", or development of convection in the model, after initialization, since convection is not initialized implicitly into the model initial fields. Currently, the only way thunderstorms will be initialized into the model, is if a large enough thunderstorm complex is captured in the initial data set, and continues to develop in the three hour assimilation procedure. Unfortunately, most of these complexes dissipate during this process, even if captured in the data field (Janish and Weiss, 1996). Because of this, a model with a faster "spin-up" time is generally preferred. Even with a faster "spin-up"

time, convection will only develop in those areas which are unstable in the model. Thus, even if convection does develop rapidly in the model, it may be in a different location than where convection is really occurring.

The data which was used to develop the BMJ scheme was derived from a tropical field experiment (Betts 1986). This scheme was developed and tested with other air masses, including an arctic airmass moving over warmer waters. However, all cases used were over water, and never over mountainous terrain. Thus, these cases all included deep moisture, especially in the lower layers, with sufficient instability leading to the development of deep convection. This differs greatly from the typical thunderstorms in the Western Region, with dry low levels, some mid-level moisture, and marginal instabilities mainly due to heating of the mountains. It appears that this difference may be somewhat to blame for the poor performance of the convective scheme in the West (Baldwin and Black, 1996, Gartner, Baldwin, and Junker 1996).

It appears that there are two likely candidates for this poor performance. The most likely is that because convection in the west is usually high-based, and not exceptionally deep, the limitation in the model that deep convection must be deeper than 290 mb may not be satisfied over higher terrain. This would explain why the parameterization appears to be better at elevations below 4000 feet, where deeper clouds are more likely to occur in the model. Thus, this grid point would be passed to the shallow convective parameterization, allowing the instability to be released without precipitation. The other candidate for potential problems with the convective scheme is that because moisture can be confined to shallow layers over the West in the summer convective season, it may not be resolved adequately with the more coarse resolution of the model mid-layers. Thus, when the convective scheme is checked, this moisture may become mixed out in such a way that the convective parameterization scheme fails. These ideas are being tested at NCEP and it is hoped that the convective prediction skill of the model over higher topography will improve once the problem is determined (M. Baldwin, personal communication).

Cumulus parameterization is far from being a simple problem, and no parameterization scheme will accurately predict the location and movement of convection. Many parameterizations suffer from the same problems as the BMJ scheme, and until model resolution becomes fine enough to implicitly resolve convection, this will continue to be a problem to the field. The next section will discuss the explicit cloud prediction scheme in the model, along with how non-convective precipitation is generated in the model.

V. THE EXPLICIT CLOUD PREDICTION SCHEME

DESCRIPTION

The primary feature of the cloud prediction scheme is the explicit calculation of cloud water and cloud ice contents in large-scale condensation processes. One predictive variable, the cloud water/ice mixing ratio, is used to represent both cloud water and cloud ice. By using one variable instead of two, model computational time and storage requirements are reduced.

Clouds are produced from large-scale condensation processes. Two three-dimensional fields are calculated: 1) cloud fraction is calculated diagnostically from relative humidity, and 2) cloud water/ice content is represented by the cloud water/ice mixing ratio. Clouds in this scheme are composed of either liquid water or ice particles, depending on the temperature (T) and the cloud top temperature (T_p). Figure 10 shows the distribution of liquid water and ice particles inside model clouds. In regions where T > 0 °C, cloud ice is not allowed to form, while in regions where T < -15 °C, cloud water cannot exist. In regions where T is between 0 °C and -15 ° C, however, the phase of any hydrometeors is determined by the cloud top temperature T_p. If T_p > -15 °C, then the cloud is assumed to consist of supercooled water. If T_p < -15 °C, which means that there are ice crystals above the layer in question, the cloud below cloud top should freeze very quickly because of seeding effects of the ice crystals into the cloud from above. Thus, the cloud is assumed to consist of frozen hydrometeors.

Cloud condensation is allowed to occur when the relative humidity of a grid box reaches a critical value, U_{00}. The value for U_{00} over land is 75%. Since condensation can more easily occur over the ocean than over land, especially in the lower atmosphere because of the abundance of available moisture, the value of U_{00} is set at 80% to avoid excess condensation.

Cloud evaporation is allowed to take place only when the relative humidity falls below the critical value of U_{00}. This is most likely to occur when clouds are advected into a drier region of the atmosphere, or when the relative humidity at a grid point, where a cloud already exists, drops below the critical value U_{00}. Evaporation will cease when the critical value of U_{00} is again reached or surpassed.

The vertical advection of clouds and hydrometeors in this scheme is neglected based on the assumption that there is an approximate balance between the small gravitational fall speed of any cloud particles and the model's large-scale vertical motions (Sundqvist et al.,1989). The horizontal advection of cloud water/ice is calculated using the same techniques as are used in the advection of specific/relative humidity in the model.

Cloud fractions derived from the cloud model are now used directly in the radiational parameterization scheme in the model. All model layer cloud fractions are used by the radiational scheme to forecast longwave and shortwave

radiation transport through the atmosphere. Previously, three layers of clouds (low--surface to 642 mb, middle--642 mb to 350 mb, and high--350 mb to 50 mb) were computed from relative humidity values and were used as input to the radiation calculations.

Precipitation in this scheme is diagnostically calculated from the cloud water/ice mixing ratio, so that once precipitation is produced from cloud water/ice, it falls to the ground through all the layers of the model below it. Snow and rain are the two forms of precipitation produced from ice clouds and liquid clouds, respectively. The interaction between snow and rain is also considered. Six major microphysical processes, which have been observed in clouds, are used in the parameterization of precipitation production from clouds. These microphysical processes are: autoconversion of cloud water to rain, collection of cloud droplets by the falling rain drops, autoconversion of ice particles to snow, collection of ice particles by falling snow, melting of snow below the freezing level, and evaporation of precipitation below cloud bases. Calculation of precipitation is done level by level, from the layer where precipitation develops to the model surface.

There are two important features in this cloud prediction scheme. First, snow melts gradually, not immediately, when it falls into a warmer portion of the cloud or atmosphere. This treatment allows the co-existence of snow and rain in some regions just below the melting level, allowing for the possibility of mixed precipitation at the model surface. Second, evaporation of precipitation occurs as it falls through the entire unsaturated layer below cloud base, and can reach the ground while it is evaporating.

The advantages of this scheme over the much more simplistic way of representing clouds solely on the basis of the relative humidity of a model atmosphere are threefold. First, it represents the hydrologic cycle much more completely, including microphysical properties inside the cloud. Second, it gives an explicit three-dimensional representation of clouds. Third, it is still simple enough to be used in operational models both in computational speed and storage. Some disadvantages of this scheme are 1) that there may be inconsistencies between the cloud water/ice mixing ratio and the cloud fraction which is calculated (since both are calculated separately), 2) some important processes, such as the advections of precipitation particles and other, more difficult to parameterize, microphysical processes are ignored, and 3) the cloud model is not initialized with any cloud/water information, thus a 'spin-up' of clouds must take place during the first few hours of integration. Additionally, since some water is tied up in the cloud water/ice in the explicit model, the relative humidity fields will be slightly lower than relative humidities in other NWP models. More information regarding this difference in relative humidities in NWP models can be found in Staudenmaier (1996). The advantages of this scheme, however, far outweigh the disadvantages, with numerous studies (Zhao, Carr and Lesins, 1991; Zhao et al., 1996; Zhao, Black and Baldwin, 1996) showing the improvements of this cloud

prediction scheme over the previously used schemes in NWP models.

The explicit cloud prediction scheme in the Eta-29 model has been shown to have improved precipitation forecasts while producing much more realistic three-dimensional model clouds and a greatly improved hydrological cycle. This has also led to slight improvements in temperature fields, wind fields, and the radiational balances in the model. Further refinement of the scheme, as discussed in Section 9, should reduce the cloud 'spin-up' problem and produce even more accurate precipitation forecasts. The next section will discuss the radiation, soil, and turbulence schemes in the Eta-29.

VI. THE RADIATION MODEL, THE SOIL MODEL, AND TURBULENCE

THE RADIATION MODEL

Radiation refers to the process of energy propagation through space, as well as the actual energy transferred. The process takes into account all the additions and subtractions of energy along a path, by an intervening medium, like water vapor or carbon dioxide. Thus, the radiation package is simply a bookkeeping method, keeping track of the energy loss due to reflection and molecular absorption along with the energy gain due to scattering in from other directions and molecular emission. In a model, the scheme keeps track of the energy at each model layer, and the can calculate whether energy is accumulating within a layer (thus raising the layer temperature), or decreasing within a layer (lowering a layer temperature). Radiative energy fluxes reaching the earth's surface drives the evolution of land surface temperature. Thus, the impact of radiation is on the model's temperature, both in the atmosphere and at the earth's surface.

Theoretically, radiative energy can come from any direction, but the largest effect is in the vertical. Thus the radiation model in the Eta-29 neglects contributions from horizontal energy propagation, and only consider the vertical energy propagation. Each component of the atmospheric medium (air) acts differently upon radiative transfer, and a great deal of information on molecular absorption, emission, and scattering has been obtained from laboratory measurements. Of course, laboratory measurements cannot exactly duplicate the effects of the real atmosphere, but for the main elements such as water vapor, carbon dioxide, ozone, and clouds, the radiation package does fairly well. Since the radiation model needs to be somewhat simple, to run quickly and efficiently, many of the other minor constituents of the atmosphere which play a role on radiative transfers are ignored.

Currently, the Eta-29 model uses a radiation package developed by the Geophysical Fluid Dynamics Laboratory (GFDL) (Fels and Schwarztkopf, 1975). Attempting to use detailed radiation physics in a numerical model would be very costly, both in time spent during integration, and in computing and storage space on the computer. Thus, a means of parameterizing these specific radiation physics into a much simpler

parameterization needed to be employed. This is what GFDL has done. In the Eta-29 model, the main elements (water vapor, carbon dioxide, ozone and clouds) are used by the parameterization to intervene in the transfer of short and longwave radiation exchange in the atmosphere. To compensate for the lack of aerosols in the model, the solar constant was reduced by three percent, to better approximate the incoming radiation. In the radiation model, water vapor is a forecast variable, whereas ozone is a zonal climatological value. Carbon dioxide is a constant value at 350 ppmv. Thus, the model, using these values, whether derived or explicitly calculated, along with simplified equations, parameterizes the exchange of energy throughout the atmosphere and at the surface. Using the cloud fraction, calculated in the cloud model at every model layer, allows the long and shortwave radiation to 'see' naturally-layered clouds as occur in the real atmosphere. This improves greatly on the three-layer clouds (low, middle, and high) used in many of the other numerical models. The specifics on this scheme are beyond the scope of this document, however testing at GFDL has shown that this scheme compares well against radiation models using a much more sophisticated radiation physics package.

THE SOIL MODEL

Over the past decade, there has been a strong push toward better modeling of land-surface processes, including heat and moisture fluxes, soil moisture evolution, snowpack treatments, and vegetation effects. Numerous papers have been published demonstrating the importance of land-surface effects on mesoscale numerical weather prediction (Mahfouf et al., 1987; Avissar and Pielke, 1989). The primary reason for this research is so that mesoscale models can realistically model the diurnal evolution and vertical structure of the planetary boundary layer. This can have direct influences on convection, precipitation, and near surface sensible weather, like temperatures and relative humidity.

In the Eta-29, a new soil model has been developed, replacing the former bucket model which used temporally fixed annual mean soil moisture values and a crude runoff treatment of moisture. The new model is an extended and enhanced version of a model developed over the last 15 years by Air Force Phillips Laboratory (Mahrt and Pan, 1984; Chen et al., 1996; Betts et al., 1996), and is referred to as the OSU or CAPS model.

The model includes physics for two soil layers, along with a vegetation canopy and snowpack. In the current configuration of the model, the soil layers are 10 cm thick (top thin layer) and 190 cm thick ("root zone" layer). The thin top layer is necessary to 1) properly treat surface infiltration/runoff response, and 2) capture the short 1-2 day drying time scales characteristic of bare soil evaporation. The thicker "root zone" layer is needed to properly simulate transpiration from the plant canopy, in particular the canopy's ability to maintain rather high rates of evaporation during the summer well after the last significant rains (2-4 week period).

A single ground surface skin temperature, T_s, is derived using the surface energy

balance equation, which represents the sum of surface energy sources/sinks from net surface solar radiation, net surface longwave radiation, total surface evaporation, surface sensible heat flux, subsurface ground heat flux, and surface heat fluxes from snowmelt. The soil temperature in the two soil layers is predicted using the traditional thermal diffusion equation, which uses a soil thermal conductivity that is a function of soil moisture and soil type. Currently there are seven soil textures in the Eta-29 model. For the lower soil temperature boundary condition at a three meter depth, the annual mean surface air temperature at the given location is used.

The total soil evaporation is the sum of three parts, 1) transpiration through the plant canopy, 2) direct evaporation from bare soil, and 3) the evaporation of standing water on the plant canopy via dew or intercepted rainfall. The time scales for the later two parts are on the scale of a few hours to a few days, however the time scale of the first part is on the order of weeks. Thus, in vegetative regions such as the Pacific Northwest, summertime surface evaporation can remain high even weeks after the last significant rainfall event due to transpiration.

The relative contributions of these three terms on the total surface evaporation is dictated primarily by the grid-cell fraction of green vegetation. This is where the Eta-29 soil model is far superior to other models. A refined data set of 0.14 degree, 5-year monthly averaged mean climatology of green vegetation fraction is used to initialize this value in the model. The monthly averaged values are interpolated to the current day of the year, for a smooth temporal trend on a daily time scale.

Together with this database, there are twelve vegetation classes used with the soil model. The bulk of the United States is covered by seven of the twelve classes: deciduous forest, evergreen forest, mixed deciduous/evergreen forest, grassland, cultivated fields, semi-arid, and desert.

Soil moisture changes in the two soil layers are governed by 1) surface infiltration of precipitation and melting snow, 2) the direct evaporation out of the ground surface or via root uptake by the plant canopy, 3) drainage working downward through the soil, and 4) hydraulic diffusivity, which can act upward or downward through the soil depending on the gradient of the vertical soil moisture. The means of how this is accomplished is beyond the scope of this document.

Finally, the soil model has an additional set of criteria for cases where there is snowcover in the model. First, the surface energy balance equation is modified to account for the possibility of snow melt. If present conditions (i.e. solar radiation and air temperature) are such that in the absence of snow, the skin temperature and the air temperature would rise above freezing, then an appropriate amount of snow is melted to match this "available" surface energy. While snow is melting, the surface skin temperature is held at 0.0 °C and the nearby 2 meter air temperature rarely rises above 2-3 °C. As the snowmelt process proceeds in time, the model

snowdepth decreases. If snowfall occurs during the model integration, the physics increase the Eta-29 snowdepth. Thus, snowcover can appear when none existed initially and initial snowcover can disappear although some existed initially. In the NGM model, both snowmelt and snowfall accumulations are absent in the model, with the initial snowcover held constant through the 48-hour model integration.

With the current method of treating snowpack in the Eta-29, there is an important limitation. The Eta model assumes complete snowcover, even for shallow or patchy snowcover. Thus, when snowcover is light, the model still holds the skin temperature at 0.0 °C which holds the 2 meter temperature near 2-3 °C, even though temperatures with light amounts of snow are not constrained to this rule in reality and may rise well above freezing. An initial fix to this problem has been to only allow this constraint to occur when the snow depth in the model reaches 2.5 inches or greater, thus allowing for temperatures to rise when snow depth is less than 2.5 inches. Forecasters will need to keep this in mind when viewing near surface temperatures under this type of situation. The complete snow algorithm will be looked at and likely restructured before next winter.

THE TURBULENCE SCHEME

The following is a very limited discussion of the turbulence scheme in the Eta-29 model. The information came from Zavisa Janjic of NCEP, a major contributor to the success of the Eta-29 model. More detailed information regarding the turbulent scheme can be found in Janjic (1994) and in Mellor and Yamada (1982).

In the Eta-29 model, the surface layer is parameterized following the similarity theory (Monin and Obukhov, 1954). This theory requires that boundary conditions in the model be prescribed at two levels in the atmosphere in order to estimate the turbulent fluxes. The values of the atmospheric variables at the lowest model level are used as the upper boundary conditions. Over open water surfaces, the values at the interface of an explicitly parameterized viscous sublayer (Janjic, 1994) and the turbulent layer are used as the lower boundary conditions. Generally, the height of the viscous sublayer is different for different variables, and depends on the flow regime. When a threshold value for friction velocity (or roughness Reynolds number) is exceeded, the viscous sublayer collapses completely, and the similarity theory is applied in the usual way, by using the surface values at the roughness height as the lower boundary condition. The integral similarity functions used over water (Lobocki, 1993) were derived from the Mellor-Yamada Level 2 turbulence closure model (Mellor and Yamada, 1982). Over land, a viscous sublayer parameterization proposed by Zilitinkevitch (1995) was implemented in order to use radiative skin temperature as the lower boundary condition instead of near surface air temperature. With this parameterization, the ratio of the roughness heights for temperature and momentum is a function of the Reynolds number. A Beljaars (1994) correction is applied in order to avoid the singularity in the case of free

convection. With this correction, a fraction of the surface buoyancy flux is converted to kinetic energy of unorganized flow near the surface, so that the friction velocity, and therefore the Monin-Obukhov length scale never vanishes.

Above the surface layer, within the planetary boundary layer (PBL) and in the free atmosphere, the Mellor-Yamada Level 2.5 second order closure scheme (Mellor and Yamada, 1982) is applied. As a result of comprehensive analysis, several modifications of this scheme have recently been introduced into the Eta models (Janjic, 1995).

The PBL height is defined as the lowest model level above the surface at which the turbulent kinetic energy (TKE) production is unable to balance the dissipation. Alternatively, the PBL height is the lowest model level above the surface at which the TKE approaches its prescribed lower bound. As before, the integral formula with Blackadar matching is used in order to estimate the master length scale within the PBL (Mellor-Yamada, 1982). The TKE production/dissipation equation is solved iteratively. In each iteration, the equation obtained by linearizing around the solution from the previous iteration is solved. Two iterations appear to be sufficient in order to achieve satisfactory accuracy.

VII. PRECIPITATION STATISTICS AND EXAMPLES

Quantitative precipitation forecasts (QPFs) from NCEP's operational model suite (Eta-48, MRF/AVN, NGM, and Eta-29) have been verified against 24-hour accumulated precipitation observations on a daily basis. Knowledge of a model's performance and biases in QPF is important for River Forecast Centers and for NWS forecast offices. This section will present seasonal statistical information regarding model performance in quantitative precipitation forecasting and show that the Eta-29 model is typically the better model for QPFs in the Western Region.

BASIC PROCEDURE

To produce a fair comparison between the model grids of 24-hour accumulated precipitation, all the models need to be interpolated to similar resolution grids. For this purpose, the Eta-29 and the Eta-48 are interpolated to the old 80 km Eta grid. The NGM model is verified on its own grid with a resolution of 80 km, while the MRF/AVN is verified on a grid of approximately 90 km resolution. The AVN model is verified for the 1200 UTC model run, while the MRF model is verified using the 0000 UTC model run. The interpolation of the Eta models is done in such a way as to conserve the total volume of water found on the original grids.

The actual accumulated precipitation observations come from a network of nearly 10,000 raingages that record 24-hour accumulated precipitation across the

lower 48 states. This data is transmitted by the River Forecast Centers around the country to NMC. The stations have a fairly dense coverage in the eastern two-thirds of the country, with more sparse coverage west of the Rocky Mountains (Fig. 11).

From the list of all possible reporting raingages, it is then determined which grid boxes will become part of the verification. Only the grid boxes that contain one or more of the network of over 10,000 raingages are considered to be part of the verification analysis domain. If a grid box does not have a routinely reporting raingage located inside it, it is not verified. The observations are analyzed to the verification grid by a simple average of all reports within a given grid box. Currently, the raingages only report when they actually receive precipitation, therefore, no observations of zero are used to compute the average. Additionally, some radar data is used to supplement rain gage reports, however this radar data is not used on any of the grid boxes which do not have a raingage data nearby for calibration.

The time periods over which the forecasts are verified are the 0-24 hour period and the 12-36 hour period. For the Eta-29, the three hour data assimilation cycle which occurs from 1200 UTC-1500 UTC and 0000 UTC-0300 UTC is used to create the 36 hour verification period. The results from both periods are combined on the attached figures. The statistics are only included if all models were available and were verified through 36 hours.

DEFINITION OF SCORES

Once the model generated QPF and the 24-hour accumulated precipitation fields are ready to be analyzed, two skill scores are computed. The scores which will be shown here are based upon comparing regions of forecast versus observed precipitation which are greater than a certain threshold, for example 0.5 inches. The two skill scores are as follows:

EQUITABLE THREAT SCORE

The equitable threat score (Schaefer, 1990) is defined as

$$\frac{(H - CH)}{(F + O - H - CH)}$$

where F = the number of grid boxes that forecast more than the threshold

O = the number of grid boxes that observe more than the threshold

H = the number of grid boxes that correctly forecast more than the threshold

CH = the expected number of correct forecasts due to chance = F*O/T

where T = the total number of grid boxes inside the verification domain

The equitable threat score seems to be a good estimate for overall forecast skill. The higher the value, the better the forecast model skill is for that particular threshold. The equitable threat score can vary from a small negative number to 1.0, where 1.0 represents a perfect forecast. This is basically the ratio of the correct forecast area to the total area of the forecast and observed precipitation. The model gets penalized for forecasting rain

in the wrong place as well as not forecasting rain in the right place. Thus, the model with the highest score is generally the model with the best forecast skill.

BIAS SCORE

The bias score is a very simple equation, defined as simply as F/O. This score does not comment at all on the skill of a model forecast in terms of the placement of precipitation, but does give an indication if a model is consistently over- or under-forecasting areas of precipitation. The best model is generally the one that remains near the 1.0 line, which means that the model does not generally over-forecast precipitation or under-forecast precipitation. If the model verifies over 1.0, it is over-predicting precipitation, and if below 1.0 it is under-predicting precipitation.

SEASONAL SCORES

Figures 12-19 are seasonal averages of the equitable threat scores and the bias scores for the previously mentioned models. The time periods for each season is as follows:

WINTER---1 DEC 1995-29 FEB 1996
SPRING---1 MAR 1996-31 MAY 1996
SUMMER---1 JUN 1996-31 AUG 1996
FALL---1 SEP 1996-27 OCT 1996*

In terms of equitable threat scores (Figs. 12,14,16,18), it can be seen that the Eta-29 typically is the best model, especially for precipitation amounts under 1.00 inches. The Eta-48 model seems to be equal to, or occasionally slightly better than the Eta-29 model for precipitation amounts over 1.00 inches, especially in the cooler seasons. The MRF/AVN model typically out performs the NGM (RAFS) model in almost all precipitation thresholds and seasons. All the models show decreasing skill with increasing precipitation threshold, with almost a steady fall in skill above 0.25 inches.

The bias scores affirm much of what was previously mentioned (Figs. 13,15,17,19). The Eta-29 repeatedly outperforms all other models, with its curve most closely following the 1.0 line. An exception to this can be seen in the Summer period, when the NGM had the better verification for precipitation under 0.50 inches. However, in precipitation amounts over 0.50 inches, the Eta-29 was clearly the better performer. The improvement in precipitation bias of the Eta-29 over the Eta-48 model can be best seen in the cool seasons, especially during the Winter period. This improvement is likely due to the improved resolution of the Eta-29 model. During the cool season, when orographic forcing by complex terrain becomes most important in the placement of heavy precipitation, the Eta-29 model clearly becomes the best model in terms of placement of precipitation (Burks and Staudenmaier, 1996; Schneider et. al, 1996; Gartner et. al, 1996).

On average, it appears that the MRF/AVN typically overestimates precipitation, while the NGM typically overestimates light amounts of precipitation while underestimating moderate amounts. The NGM appears to be the worse model overall in forecasting heavy amounts of precipitation. The Eta-48/Eta-29 models appear to suffer the same biases of

overestimating light precipitation amounts and underestimating heavier precipitation amounts, with the Eta-29 showing some improvement in these biases over the Eta-48 model.

The Eta-29 model has shown many times that it can predict previously unresolvable sub-synoptic features important to several key forecast situations. At the Hydrometeorological Prediction Center, the Eta-29 has proven to be a valuable tool (Schneider et. al, 1996). Model resolution of terrain and mesoscale structure within cool season extratropical systems have contributed to substantial improvements over previous NCEP regional models. This improvement in QPF guidance generated by the Eta-29 was also described in a paper by Burks and Staudenmaier (1996) in relation to the 'Storm of the Decade' which hit the Western United States in December 1995.

The Eta-29 model has also shown considerable improved skill in the arena of severe weather. At the same time that Western Region was evaluating the Eta-29 model, the National Severe Storms Laboratory (NSSL) in cooperation with the Storm Prediction Center (SPC) also participated in a real-time evaluation of the model. This evaluation focused on various mesoscale phenomena associated with forecasting severe convection, in particular the low-level jet and dryline in the southern Plains of the United States (Janish and Weiss, 1996). It was found that in many cases, the Eta-29 model was able to resolve mesoscale structures providing enhanced guidance beyond that typically available from other operational NWP models. The model did, however, have problems resolving features such as outflow boundaries and triple points along the dryline. Similar results were also discussed in a paper describing the performance of the Eta-29 model in determining the environment and development of a bow echo in California (Staudenmaier, 1996). It was found that the Eta-29 did well in detecting the development of convection, along with the organization of the precursor elements which led to the development of the bow echo complex. However, due to the parameterization of convection, the model did not develop the meso-scale features which led to the severity of the bow echo and the high winds associated with the boundary.

These examples underscore the fact that the Eta-29 model is improving the ability of forecasters in the field to make better forecasts. The model may not yet have the resolution to explicitly forecast certain events, but many of the precursor elements leading up to these events are now being forecast by the model. The next section will discuss the future of the model, and some of the improvements which are expected over the next few years.

VIII. THE FUTURE OF THE ETA-29 MODEL

Even with all the problems discussed in this document, in the parameterizations and in the way data is assimilated into the model, the Eta-29 still manages to capture much of the details of the day to day weather pattern. Due to its finer resolution, the Eta-29 is likely the model

that does assimilate the most data of any of the other models in the NCEP suite. Modelers are now at a crossroads in terms of the philosophy of data assimilation and parameterizations. Up to this point, due to the poor resolution of the models, the boundary layer was never really that important, as the model tended to wipe out any detail soon into the integration and create its own 'model' PBL. Real surface data had little importance in the model, since at coarse resolution, both in the vertical and the horizontal, any pertinent information from real surface data would be quickly washed out during the model integration. Now, however, with finer resolution, and a much more resolved planetary boundary layer, the need for actual surface information in the model is becoming more and more of a necessity. Forecasters were not presented with surface temperature, relative humidities, and surface winds until the Eta-29 appeared. This is the first time that forecasters have a model with fine enough resolution to be able to start using the boundary layer information as a forecasting tool. However, much of the information near the surface is not very accurate, and modelers will now have to look for ways to improve the mesoscale boundary layer forecasts, just as they have worked in the past to improve the skill of the AVN, NGM and Eta models in forecasting synoptic scale features. Work on various parameterizations will also have to occur, as many of these schemes were designed for synoptic scale processes, not mesoscale ones.

The modelers at NCEP are looking at improving the skill of the Eta-29 through a variety of ways over then next two years. Most importantly, the assimilation process of the Eta-29, which currently is only a three hour assimilation using the first guess from the GDAS, will be changed so that it cycles on itself, and the assimilation will last six hours rather than three. Thus, the information used to initialize the model will come from the Eta-48 as opposed to the coarser resolution GDAS. A first guess generated from the same model is preferable to one based on a global spectral model-based first guess because of the matching physics, the better resolution, and less of a 'spin up' problem. This will allow many of the physical models, like the soil model, the cloud model, and the radiation model, to have initial values from the previous run, rather than having to initialize with zero information and 'spin up' to reality.

Another change to the assimilation process will be with the method used in creating the initialization for the model. NCEP plans to go from the current OI analysis technique to a newer and potential better method, the 3-dimensional variational analysis technique (3DVAR). OI and 3DVAR are actually two methods for solving the same problem, which is finding the best fit of both observational data and the model first guess forecast. The formal mathematical solution to this problem involves the solution of a matrix problem of dimension equal to the number of observations, which is impractically large. The OI procedure for solving this problem has been to make a local approximation, by using a small number (30-100) of nearby observations to compute smaller matrices at each grid point. Because of the way the OI procedure works, it has

only been possible to use observations directly related to model variables, as mentioned above.

The 3DVAR method for solving this matrix problem makes no local approximation. The entire matrix problem is solved. Two procedures make this possible. First, the matrix being solved for is not computed directly, but instead is represented by a sequence of simple operations. Second, the problem is solved by iteration, using a technique known as the conjugate gradient method. One of the main advantages of using the 3DVAR technique is that observations no longer need to be the same as model variables. It is only necessary to have a procedure which can compute a simulated observation from standard model variables. This is called the forward model. For example, a radial wind measurement from a doppler radar is only a partial measurement of the wind, along the direction of the radar beam. The forward model in this case is simply the projection of the model wind along the beam direction at the observed location. Thus, the 3DVAR system will be much more flexible than the OI technique and will make it possible to use many new data sources and will better utilize existing data.

The cloud model will also be initialized with data in the future, through the use of real-time, high-resolution nephanalyses (cloud maps), and hourly raingage data over the U.S. These will be used to initialize the cloud water/ice, moisture and latent heating fields to be internally consistent with observed precipitation rates. Also, with the cycling EDAS system during the assimilation process, and a longer assimilation period, the model will have cloud water/ice values to initialize with, and more time to 'spin up' to reality. This should have a positive impact on precipitation scores, along with more realistic cloud fields. This process will also be used to moisten the soil model, thus improving evaporation and boundary layer moisture fields. Because of the 3DVAR system, it will also be possible to use cloud observations inferred from the GOES satellite to help initialize the cloud model.

Additional sources of satellite data are expected to be used more often in the future as well. Current GOES 8/9 moisture profiles are now accurate enough that the resulting integrated layer precipitable water values are good enough to be of use in the model. Black-body radiance temperature information from the satellite is also expected to be used to initialize the model once the 3DVAR technique is implemented. Satellite soundings still do not have enough resolution to be of use in the assimilation process, although in the future, it is hoped they will improve to the point of being useful for initializing the model in data sparse regions, especially over the oceans.

NCEP has also developed a smaller-scale model with a resolution of 10 km, hereafter called the Eta-10. This model, with much more resolved topography in the Western Region, should allow for some more surface data to be used in the assimilation process, although how much more will make it into the model is not yet known. To produce useful forecasts at such small grid spacing, it will be more critical than ever to initialize the model

with mesoscale information, both to allow the model to be more accurate, and to allow the boundary layer to evolve realistically. At high resolution, parameters such as current vegetation type and percentage along with soil type play a crucial role in the soil moisture pattern, which is reflected in boundary layer processes. Thus, much higher resolution and real-time data will need to be found to initialize the model with, rather than the current climatological values. The Eta-10 is being tested during the first part of 1997 over the Western Region domain. It is likely to show additional improvements in numerical modeling similar to those of the Eta-29 model over the Eta-48 model.

Doppler winds from the NEXRAD network are also being examined for as sources of mesoscale initialization in the Eta-10. This data set can only be used once the 3DVAR analysis technique is implemented, as mentioned above. This is because the wind measurements are incomplete, with only the component along the radar beam being measured. Conventional methods, like OI, require overlapping beams from two radars to get the full wind vector. In the NEXRAD network, there are not many locations with such a set-up. With the 3DVAR method, the along-beam component of the wind can be used, rather than the complete wind vector. More information regarding the use of Doppler winds in the initialization of the Eta-10 can be found in Parrish et. al, 1996. Local mesoscale networks of surface observations will also be used in the future, assuming that they are not thrown out during the assimilation process.

IX. SUMMARY AND CONCLUSIONS

The original purpose of the Eta-29 model was to 'augment the current array of operational synoptic-scale numerical forecasts with guidance down to mesoscale ranges' (Black, 1994). Clearly, the Eta-29 model has lived up to every expectation with superior forecasts and sub-synoptic detail. Perhaps it does not capture all the mesoscale events that one could expect a model of its resolution to capture, but it still represents a huge step forward in numerical modeling--to generate operational mesoscale forecasts across the 48 contiguous states. Thanks to feedback from field forecasters and others, along with a willingness of NCEP to push the envelope of technology and modeling in response to this feedback, the National Weather Service has gained an exceptional forecasting tool which has already proven itself in lives and property saved through improved forecasts. The future continues to look bright, with the possibility of even higher resolution models becoming operational.

X. REFERENCES

Arakawa, A., and V.R. Lamb, 1977: Computational design of the basic dynamical processes of the UCLA general circulation model. *Methods Comput. Phys.*, **17**, 173-265.

Avissar, R., and R. Pielke, 1989: A parameterization of heterogeneous land surfaces for atmospheric numerical models and its impact on regional meteorology. *Mon. Wea. Rev.*, **117**, 2113-2136.

Baldwin, M.E., and T.L. Black, 1996: Precipitation forecasting experiments in the western U.S. with NCEP's mesoscale Eta model. *Preprints, 11th Conf. on Num. Wea. Pred.*, AMS, Norfolk, VA. Aug, 1996.

Beljaars, A.C.M., 1994: The parameterization of surface fluxes in large-scale models under free convection. *Quart. J. Roy. Meteor. Soc.*, **121**, 255-270.

Betts, A.K., 1982: Saturation point analysis of moist convective overturning. *J. Atmos. Sci.*, **39**, 1484-1505.

Betts, A.K., 1986: A new convective adjustment scheme. Part I: Observational and theoretical basis. *Quart. J. Roy. Meteor. Soc.*, **112**, 677-691

Betts, A.K., and M.J. Miller, 1986: A new convective adjustment scheme. Part II: Single column tests using GATE wave, BOMEX, and arctic air-mass data sets. *Quart. J. Roy. Meteor. Soc.*, **112**, 693-709.

Betts, A., F. Chen, K. Mitchell, Z. Janjic, 1996: Assessment of land-surface and boundary-layer models in 2 operational versions of the Eta model using FIFE data. (*Accepted in Mon. Wea. Rev.*)

Black, T.L., 1994: The new NMC mesoscale Eta model: Description and Forecast Examples. *Wea. Forecasting*, **9**, 265-278.

Burks, J.E., and M.J. Staudenmaier, 1996: A comparison of the Eta and the Meso Eta models during the 11-12 December 1995 storm of the decade. *WR-Technical Attachment **96-21***.

Chen, F., K. Mitchell, J. Schaake, Y. Xue, H. Pan, V. Koren, Y. Duan, M. Ek, and A. Betts, 1996a: Modeling of land-surface evaporation by four schemes and comparison with FIFE observations. *J. Geophys. Res.*, **101**, D3, 7251-7268.

Chen, F., Z. Janjic, K. Mitchell, 1996b: Impact of atmospheric surface layer parameterization in the new land-surface scheme of the NCEP mesoscale Eta numerical model. (*Submitted to Boundary-Layer Meteor.*)

Fels, S.B., and M.D. Schwarztkopf, 1975: The simplified exchange approximation: A new method for radiative transfer calculations. *J. Atmos. Sci.*, **32**, 1475-1488.

Gartner, W.E., M.E. Baldwin, and N.W. Junker, 1996: Regional analysis of quantitative precipitation forecasts from NCEP's early Eta and Meso-Eta models. *Preprints, 15th Conf. on Weather Analysis and Forecasting*, AMS, Norfolk, VA. Aug, 1996.

Janish, P.R. and S.J. Weiss, 1996: Evaluation of various mesoscale phenomena associated with severe convection during VORTEX-95 using the Meso Eta model. *Preprints, 15th Conf. on Weather Analysis and Forecasting*, AMS, Norfolk, VA. Aug, 1996.

Janjic', Z.I., 1994: The step-mountain eta coordinate model: Further developments of the convection, viscous sublayer, and turbulence closure schemes. *Mon. Wea. Rev.*, **122**, 927-945.

Janjic', Z.I., 1995: The realizability of the Mellor-Yamada Level 2.5 turbulence closure model under strong forcing. *Summer School in Meteorology: Hydrological Cycle in Atmospheric Models, Federal Hydrometeorological Institute*, 28 August-8 September 1995, Krivaja-Backa Topola, Yugoslavia, Doc. 8.

Lobocki, L., 1993: A procedure for the derivation of surface-layer bulk relationships from simplified second-order closure models. *J. Appl. Meteor.*, **32**, 126-138.

Mahfouf, J.F., E. Richard, and P. Mascart, 1987: The influence of soil and vegetation on the development of mesoscale circulations. *J. Clim. Appl. Meteor.*, **26**, 1483-1495.

Mahrt, L., and H.L. Pan, 1984: A two-layer model of soil hydrology. *Boundary-Layer Meteor.*, **29**, 1-20.

Mellor, G.L., and T. Yamada, 1974: A hierarchy of turbulence closure models for planetary boundary layers. *J. Atmos. Sci.*, **31**, 1791-1806.

-------, and -------, 1982: Development of turbulence closure models for geophysical fluid problems. *Rev. Geophys. Space Phys.*, **20**, 851-875.

Mesinger, 1984: A blocking technique for representation of mountains in atmospheric models. *Riv. Meteor. Aeronaut.*, **44**, 195-202.

Monin, A.S., and A.M. Obukhov, 1954: Basic laws of turbulent mixing in the surface layer of the atmosphere. Contrib. *Geophys. Inst. Acad. Sci.* USSR, (151), 163-187 (in Russian).

Parrish, D., J. Purser, E. Rogers, and Y. Lin, 1996: The regional 3D-variational analysis for the Eta model. *Preprints, 11th AMS Conf. on Numerical Weather Prediction,* Norfolk, VA. Aug, 1996.

Schaefer, J.T., 1990: The critical success index as an indicator of warning skill. *Wea. Forecasting*, **5**, 570-575.

Schneider, R.S., N.W. Junker, M.T. Eckert, and T.M. Considine, 1996: The performance of the 29 km Meso Eta model in support of forecasting at the Hydrometeorological Prediction Center. *Preprints, 15th Conf. on Weather Analysis and Forecasting*, AMS, Norfolk, VA. Aug, 1996.

Staudenmaier, M.J., 1996: A description of the Meso Eta model. *WR-Technical Attachment* **96-06**.

Staudenmaier, M.J., 1996: An evaluation of the performance of the Meso-Eta model on a dynamic cold season bow echo in California. *WR-Technical Attachment* **96-12**.

Staudenmaier, M.J., 1996: Differences in relative humidities in the NMC model suite. *WR-Technical Attachment* **96-20**.

Staudenmaier, M.J., 1996: Precipitation verification statistics from the NCEP operational modelsuite. *WR-Technical Attachment* **96-28**.

Staudenmaier, M.J., 1996: The explicit cloud prediction scheme in the Meso Eta model. *WR-Technical Attachment* **96-29**.

Staudenmaier, M.J., 1996: The initialization procedure in the Meso Eta model. *WR-Technical Attachment* **96-30**.

Sundqvist, H., E. Berge, and J.E. Kristjansson, 1989: Condensation and cloud studies with a mesoscale numerical weather prediction model. *Mon. Wea. Rev.*, **117**, 1641-1657.

Swanson, R.T., 1995: Evaluation of the mesoscale Eta model over the western United States. Masters Thesis, University of Utah, 113 pp.

Zhao, Q., F.H. Carr, and G.B. Lesins, 1991: Improvement of precipitation forecasts by including cloud water and cloud ice into NMC's Eta model. *Preprints, 9th Conference on Numerical Weather Prediction, Denver Colorado.*

Zhao, Q., T.L. Black, G.J. DiMego, K. Mitchell, and F. Chen, 1996: Improved clouds and their impact on radiation calculation in the Eta model at NCEP. *Preprints, 11th AMS Conference on Numerical Weather Prediction, Norfolk, VA.*

Zhao, Q., T.L. Black, and M.E. Baldwin, 1996: Implementation of the cloud prediction scheme in the Eta model at NCEP. Submitted to *Weather and Forecasting.*

Zilitinkevitch, S.S., 1995: Heat and mass transfer in the convective surface layer. *J. Atmos. Sci.*, **52**, (in press).

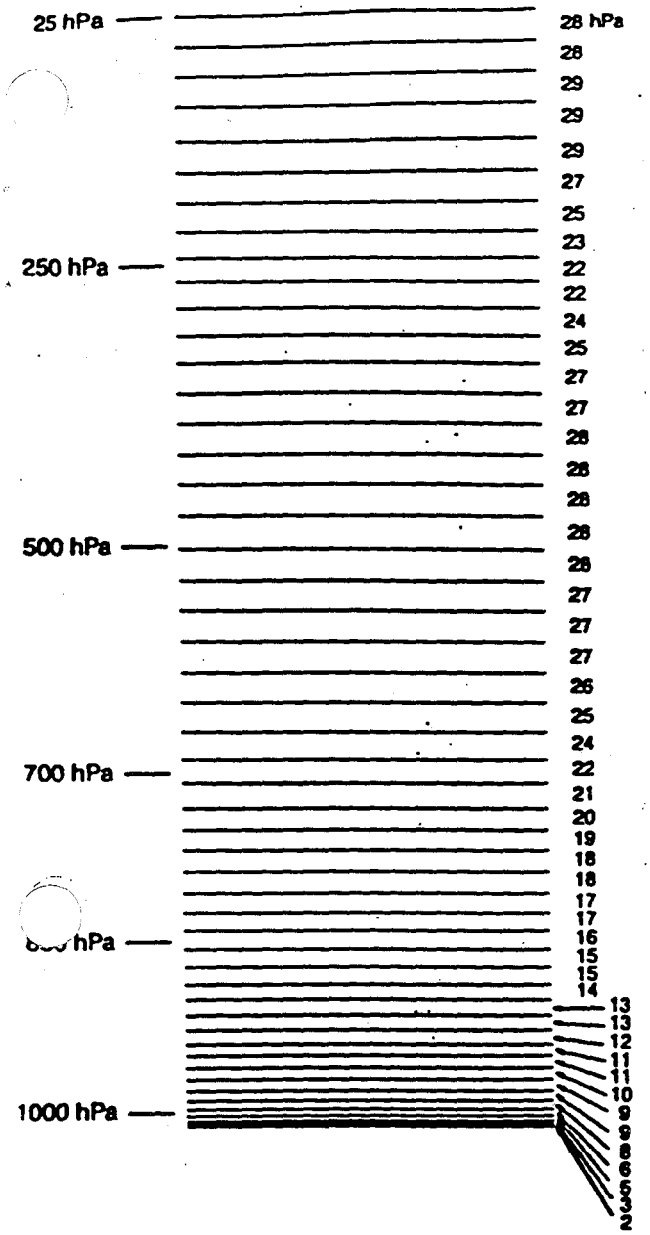

FIG. 1. A sample distribution of the 50 layers in the mesoscale Eta Model. The pressures on the left side indicate the layers' positions with respect to the standard atmosphere, while the numbers on the right give the approximate pressure depth of each layer in hectopascals.

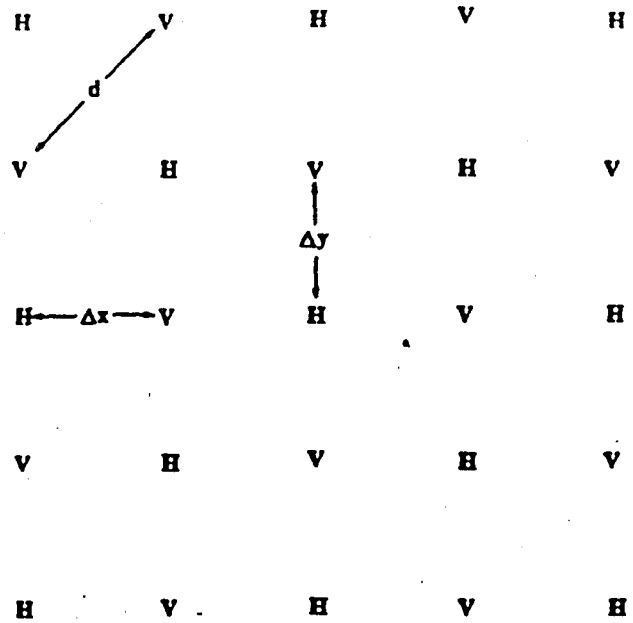

FIG. 2. A subset of the model's Arakawa E grid. Each "H" represents a mass variable, while each "V" represents both horizontal wind components. The values Δx and Δy are the grid increments in the model's rotated latitude–longitude space, while the distance "d" indicates the resolution.

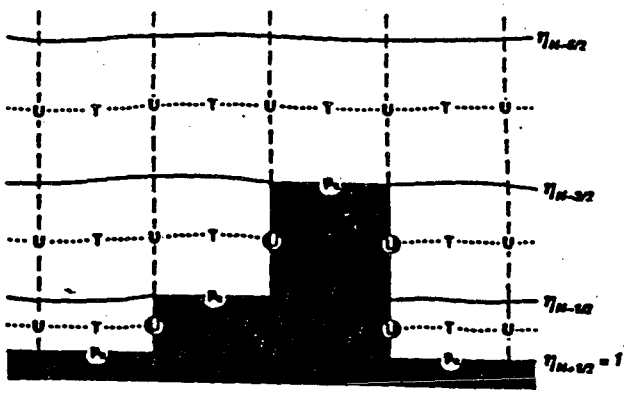

FIG3 An idealized vertical cross section of the model's step topography. Each T indicates a "mass" variable within each grid box, while each U represents both horizontal wind components. The quantity p_s is the surface pressure. The circled U's on the sides of steps indicate wind points that are defined as zero at all times.

Figure 4: Map of the western United States showing those areas most likely to have surface observations included in the Eta-29 data assimilation process (shaded areas).

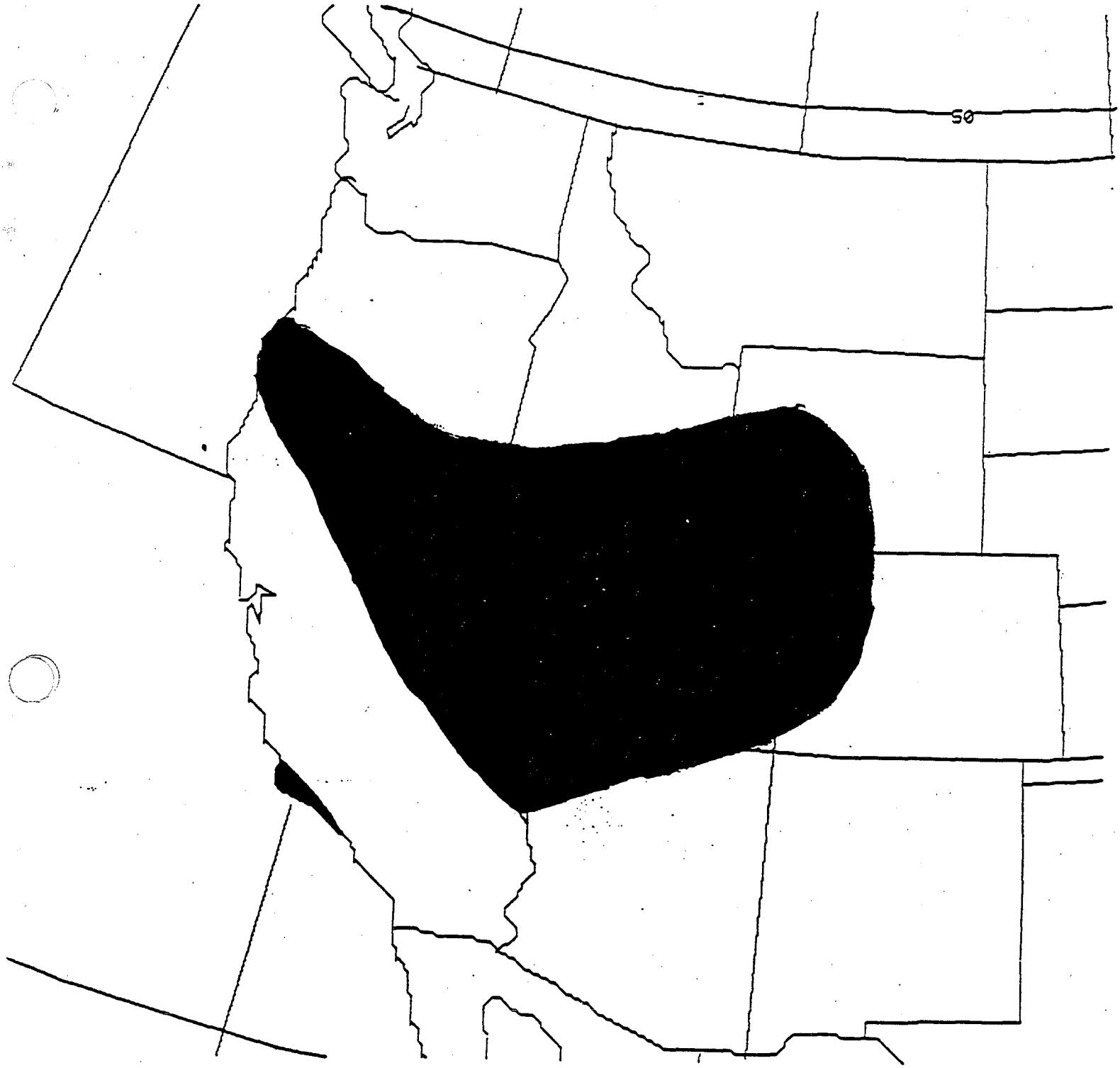

Figure 5: Map of the western United States showing those areas most likely to have data loss of more than 20 mb in the lowest portion of radiosonde data in the Eta-29 assimilation process (shaded areas).

STATION IDENTIFICATION	ETA (MB)	MSO (MB)
72582 LKN	29	21
72376 FGZ	0	18
72274 TUS	60	13
72572 SLC	59	68
72597 MFR	109	48
72493 OAK	18	15
72489 REV	36	46
72293 SAN	12	5
72387 DRA	42	29
72476 GJT	98	105
72576 RIW	104	27
72786 GEG	4	11
72776 GTF	26	4
72797 UIL	14	9
72694 SLE	50	15
72681 BOI	55	21
72768 GGW	29	13
72393 VBG	5	32
72381 EDW	12	4

Figure 6: Table of western United States radiosonde sites showing the average depth of data loss of the lowest portion of the raob in both the Eta-48 model (ETA) and the Eta-29 model (MSO) for the period of 12-15 November 1996. Values are likely similar throughout the year.

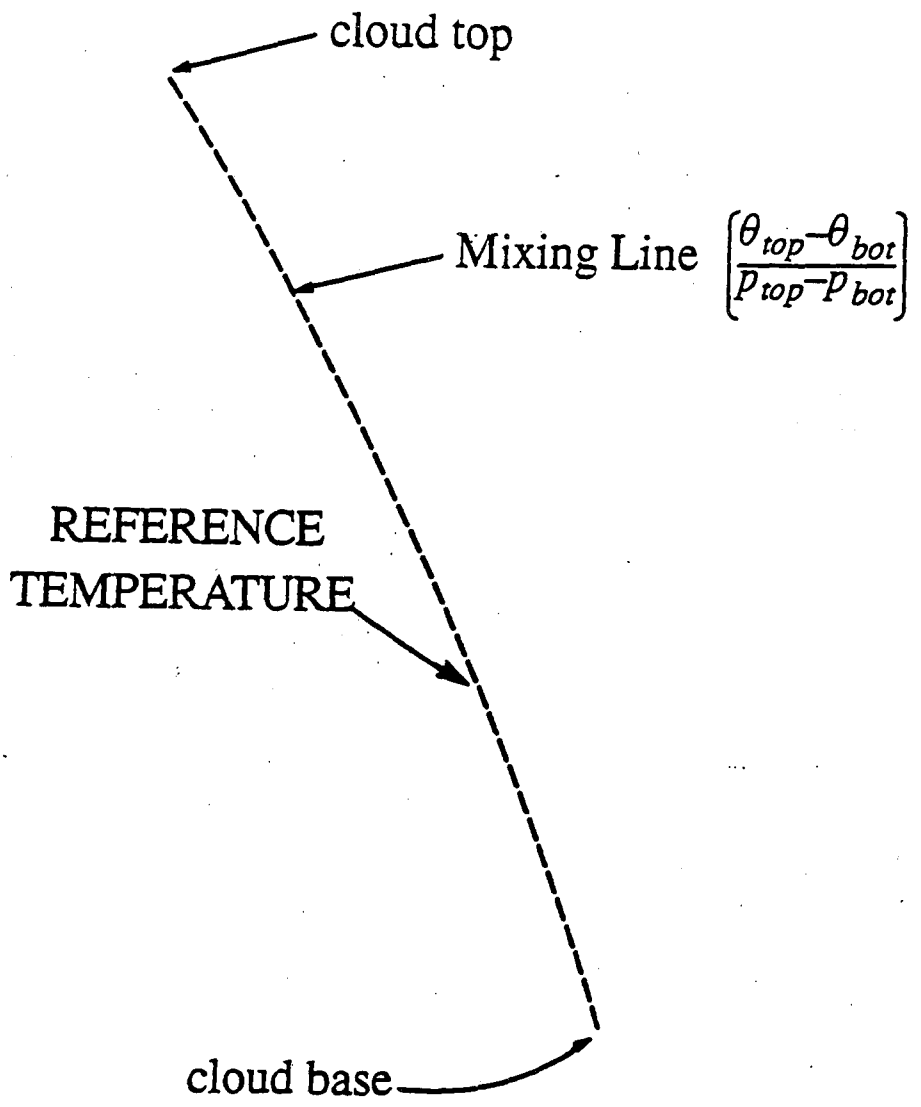

Figure 7: Diagram showing the construction of the mixing line used in the determination of shallow convection in the Eta-29 model.

Construction of 1st Guess Temperature Reference Profile for Deep Convection

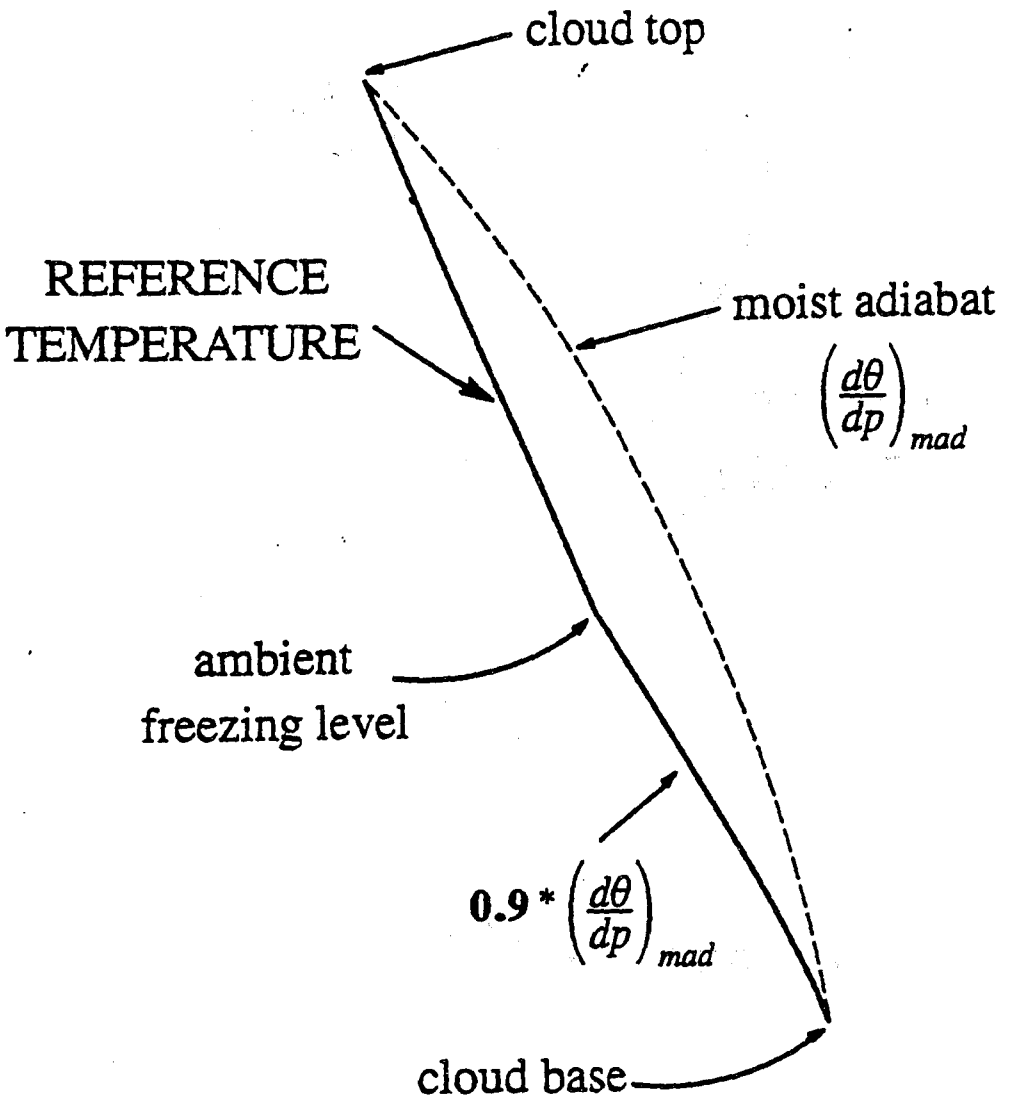

Figure 8: Diagram showing the construction of the reference temperature profile used in the determination of deep convection in the Eta-29 model.

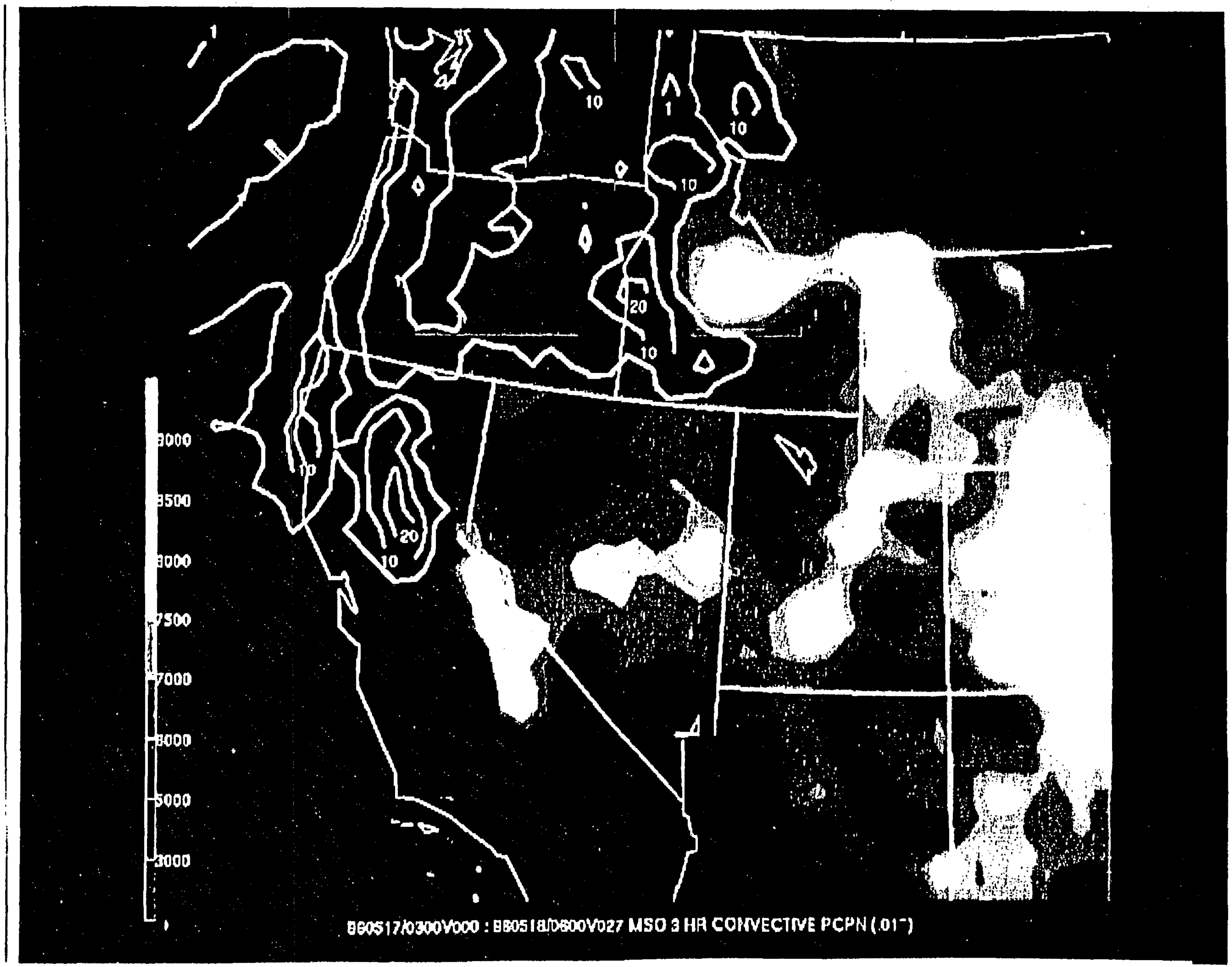

Figure 9: An example of a typical three hour convective precipitation accumulation graphic illustrating the lack of convective precipitation over mountainous terrain over 4000 feet in

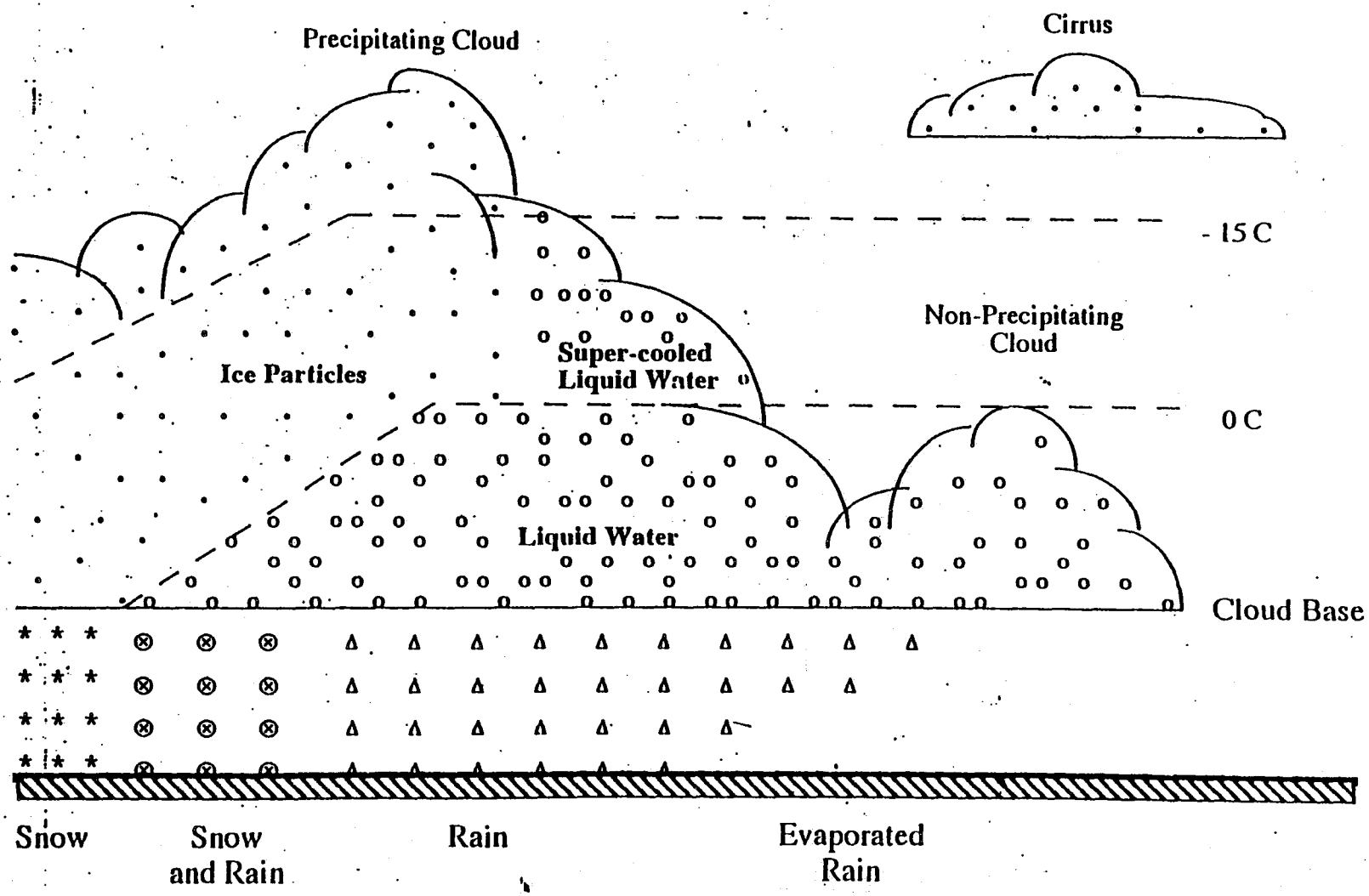

Figure 10: Diagram showing the distribution of liquid water and ice particles inside model clouds in the Eta-29 model.

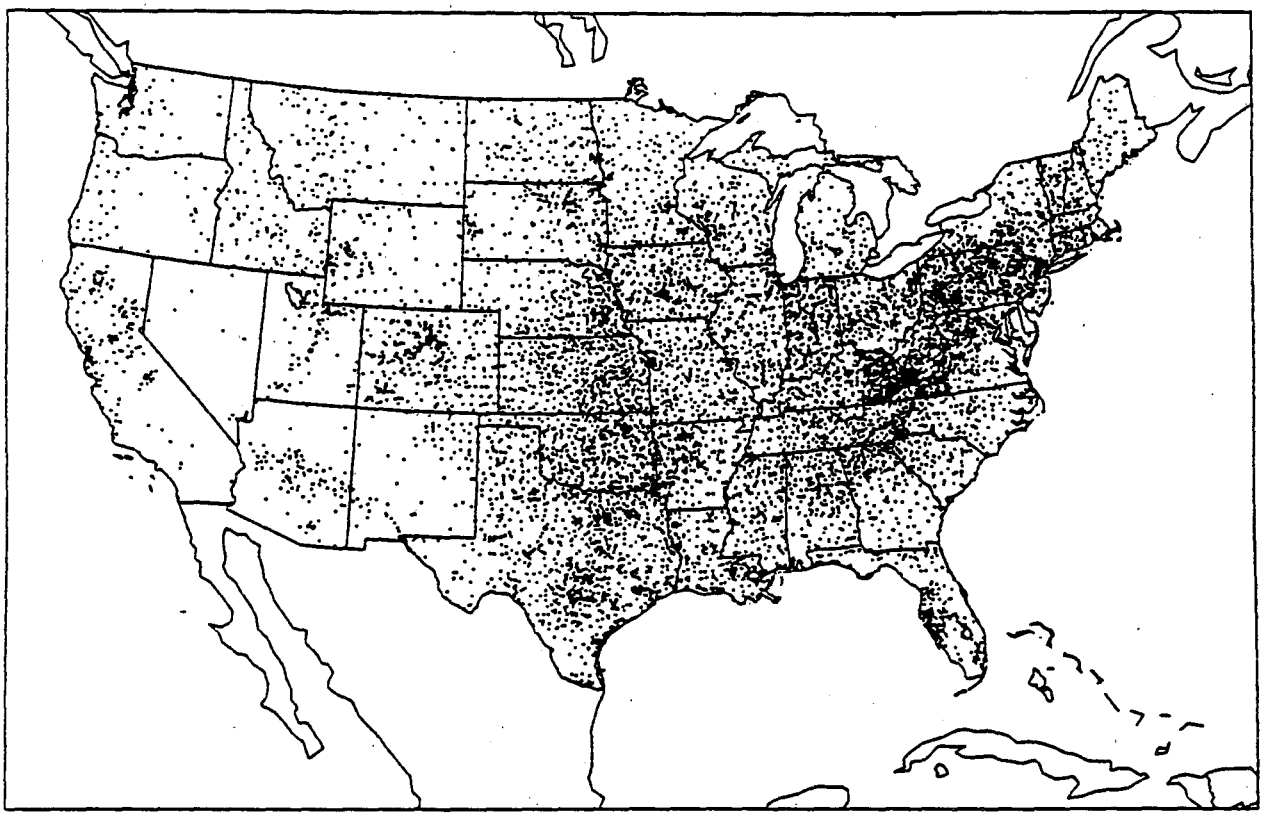

Figure 11: Diagram showing the network of 24-hour accumulated precipitation stations located over the lower 48 states.

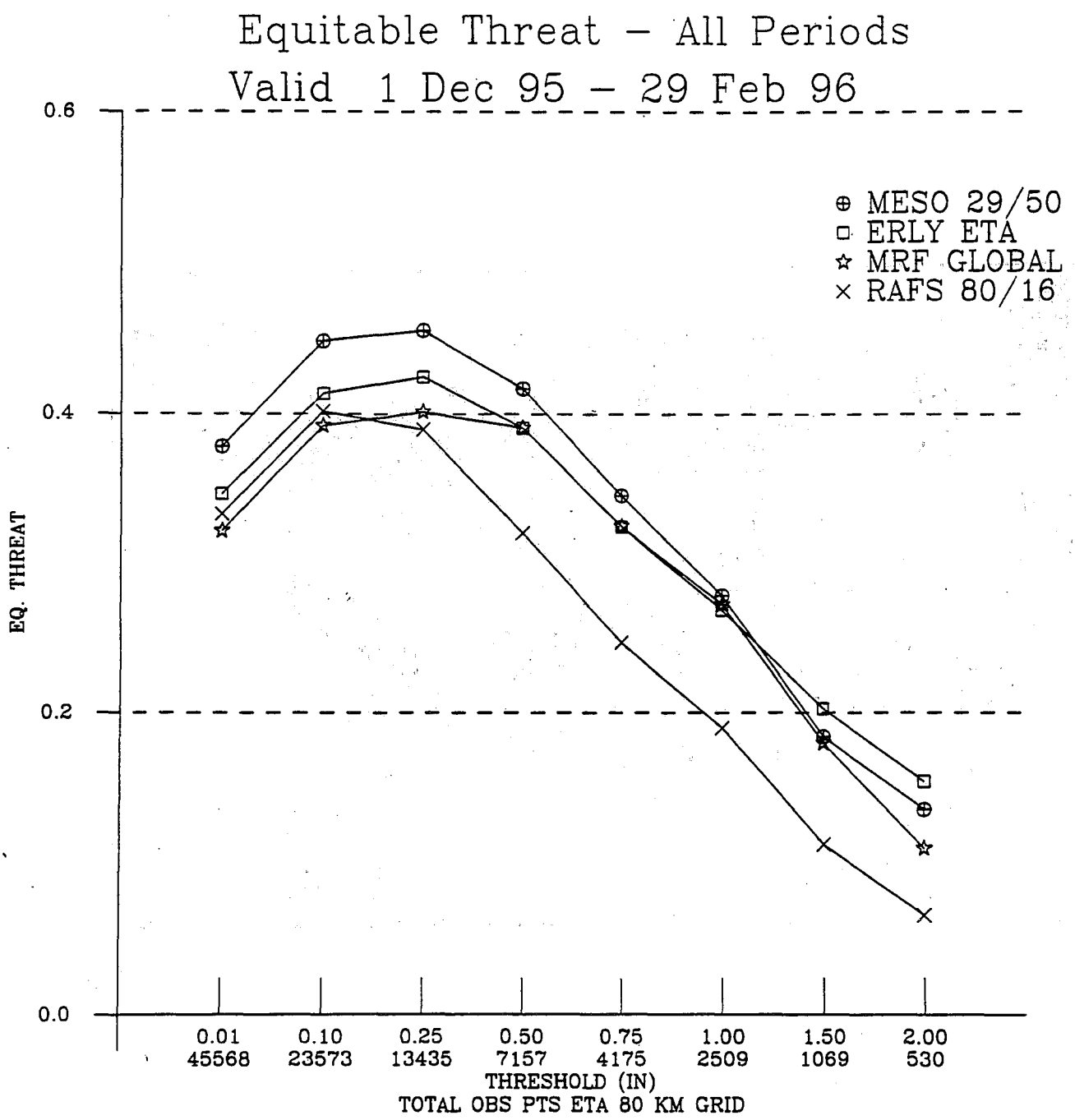

Figure 12: Equitable threat scores for all forecasts during the period 1 December 1995 - 29 February 1996.

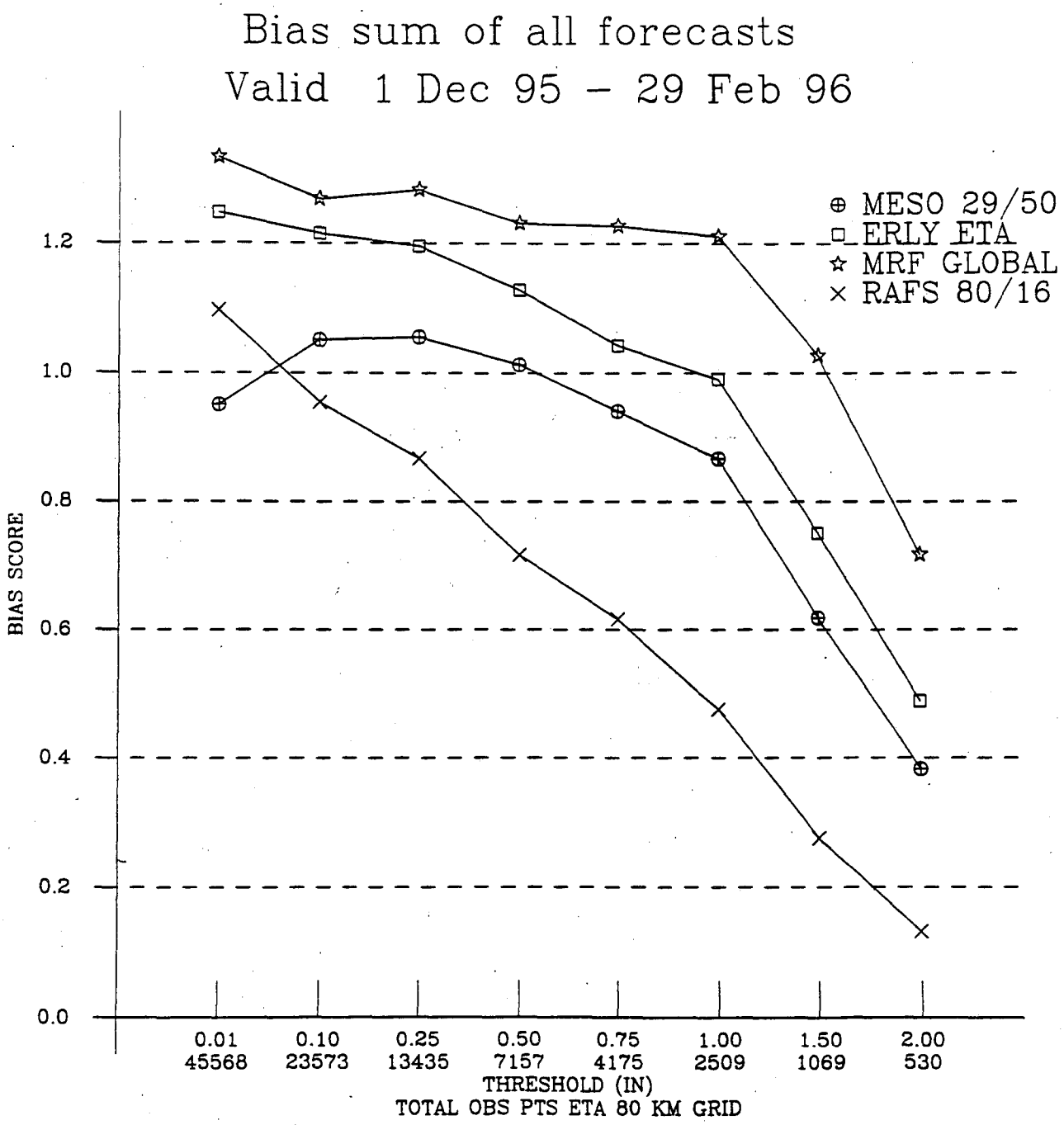

Figure 13: Bias sum scores for all forecasts during the period of 1 December 1995 - 29 February 1996.

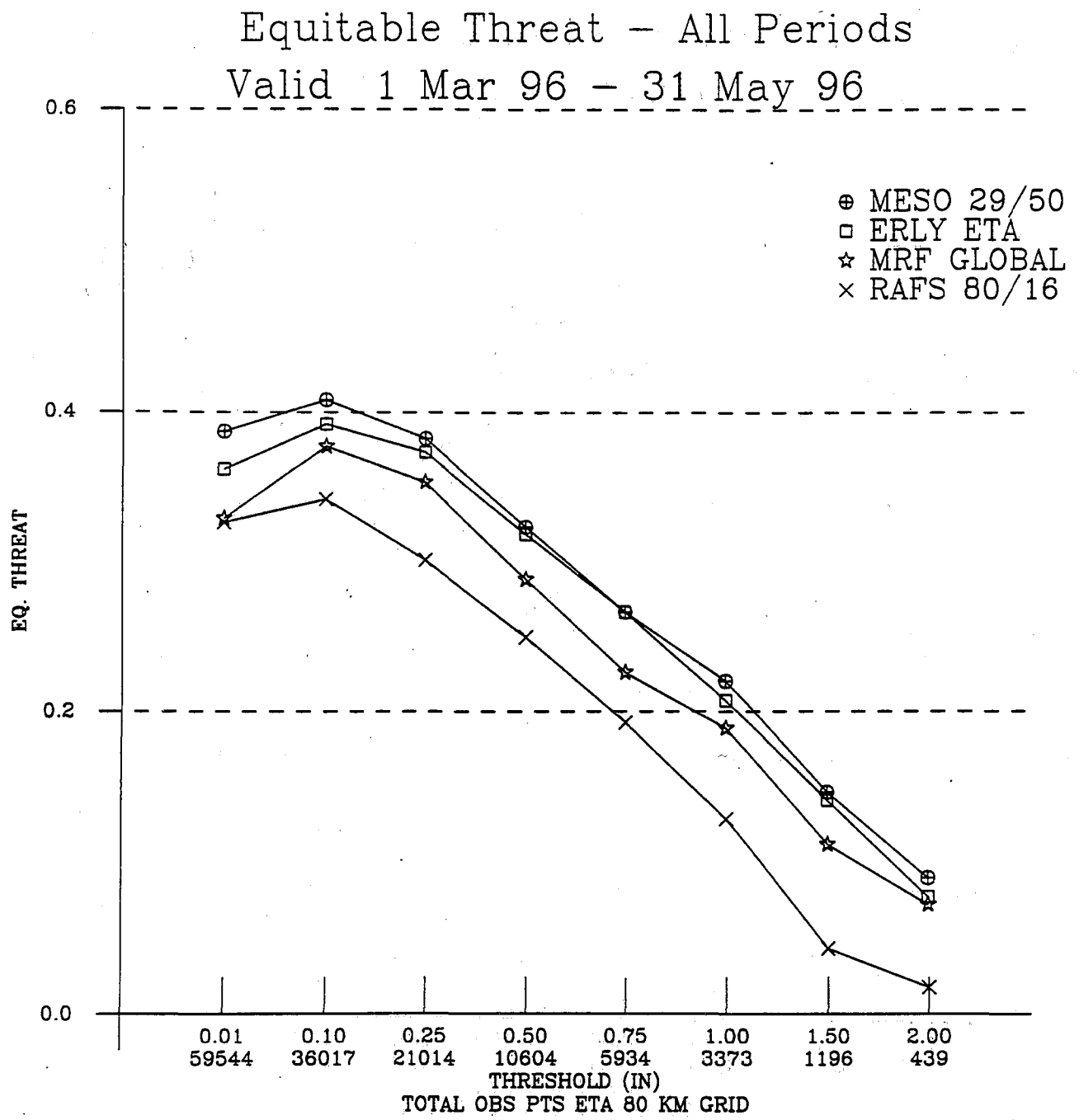

Figure 14: Equitable threat scores for all forecasts during the period 1 March - 31 May 1996.

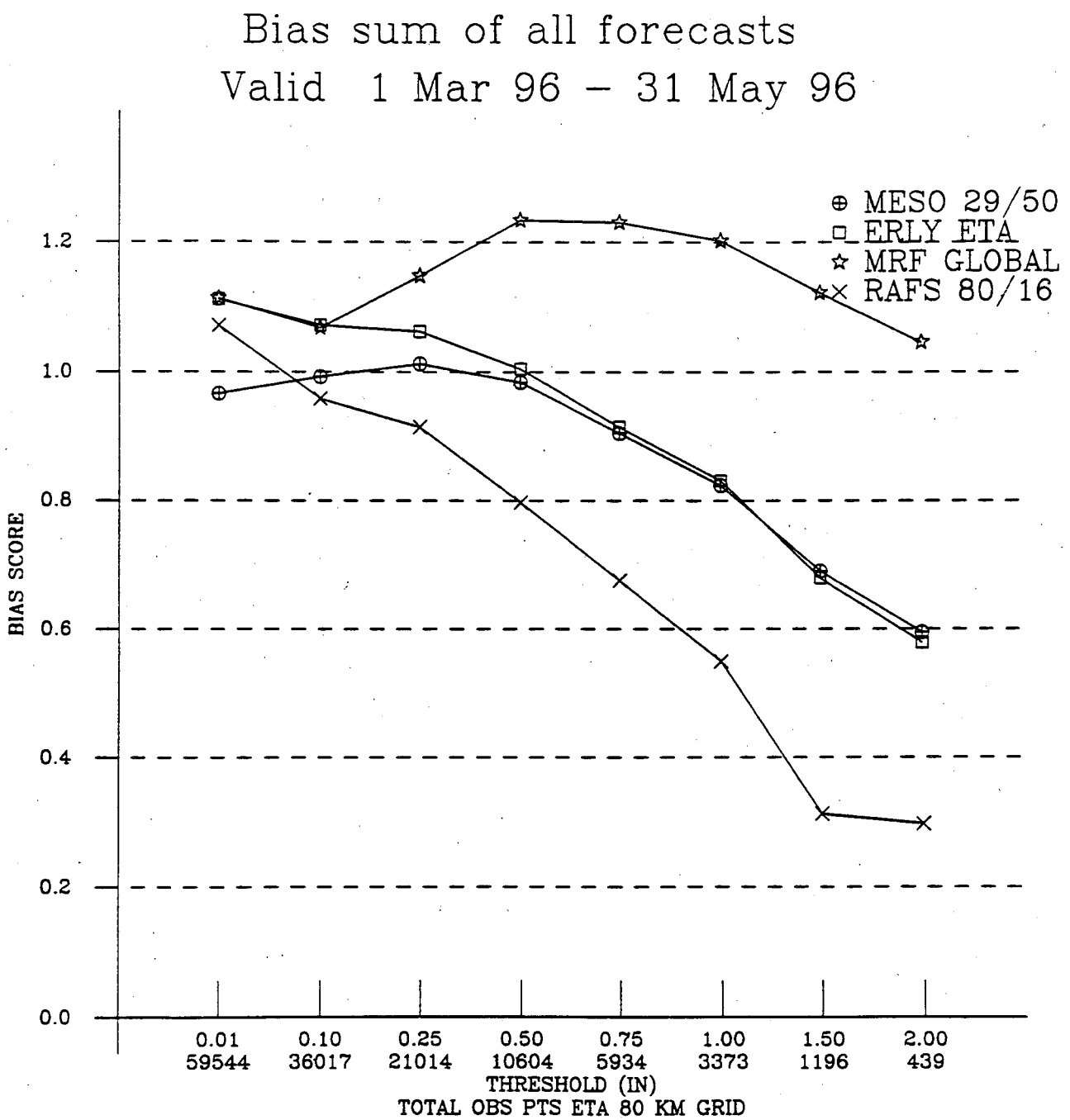

Figure 15: Bias sum scores for all forecasts during the period of 1 March - 31 May 1996.

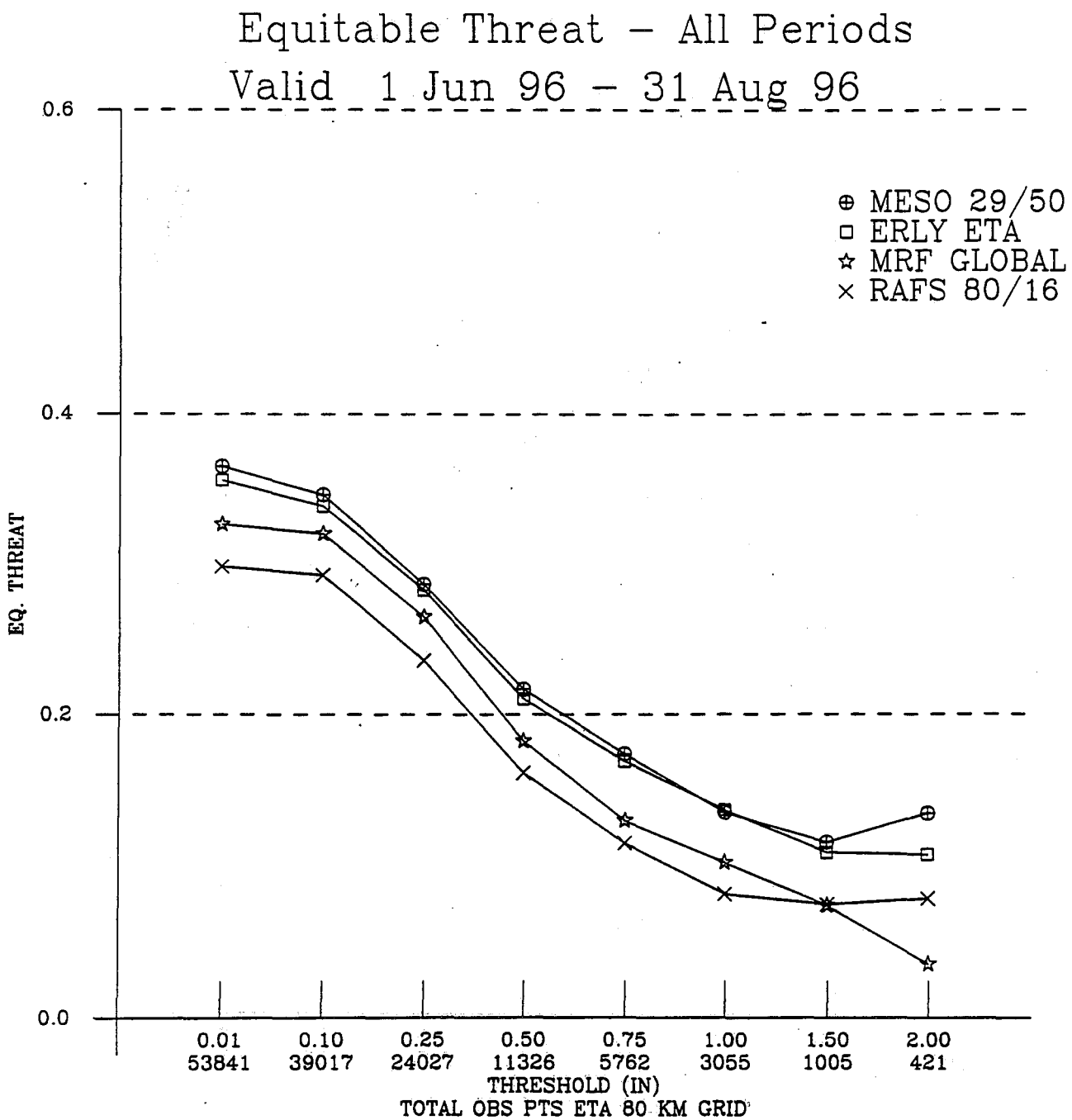

Figure 16: Equitable threat scores for all forecasts during the period 1 June - 31 August 1996.

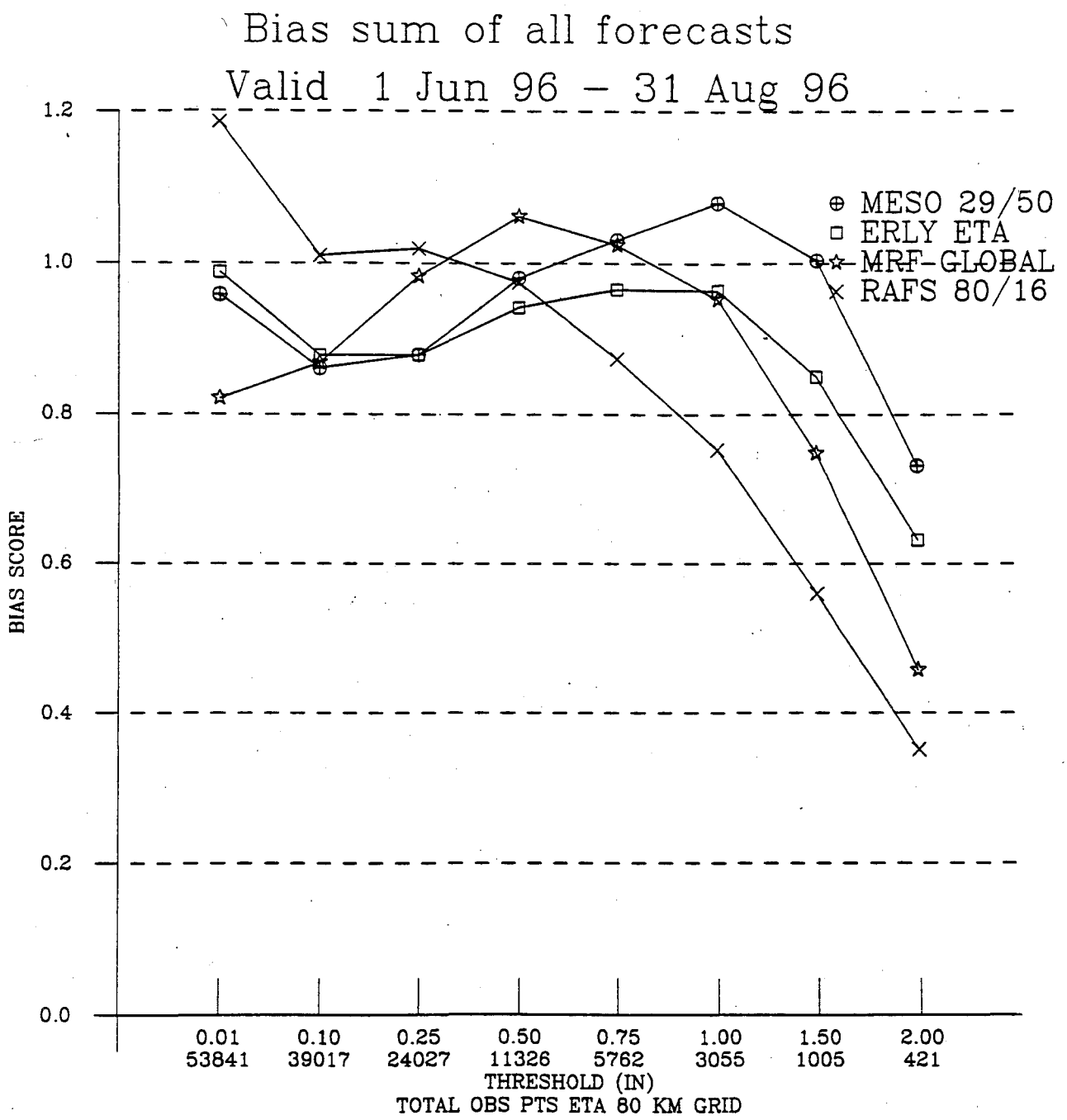

Figure 17: Bias sum scores for all forecasts during the period of 1 June - 31 August 1996.

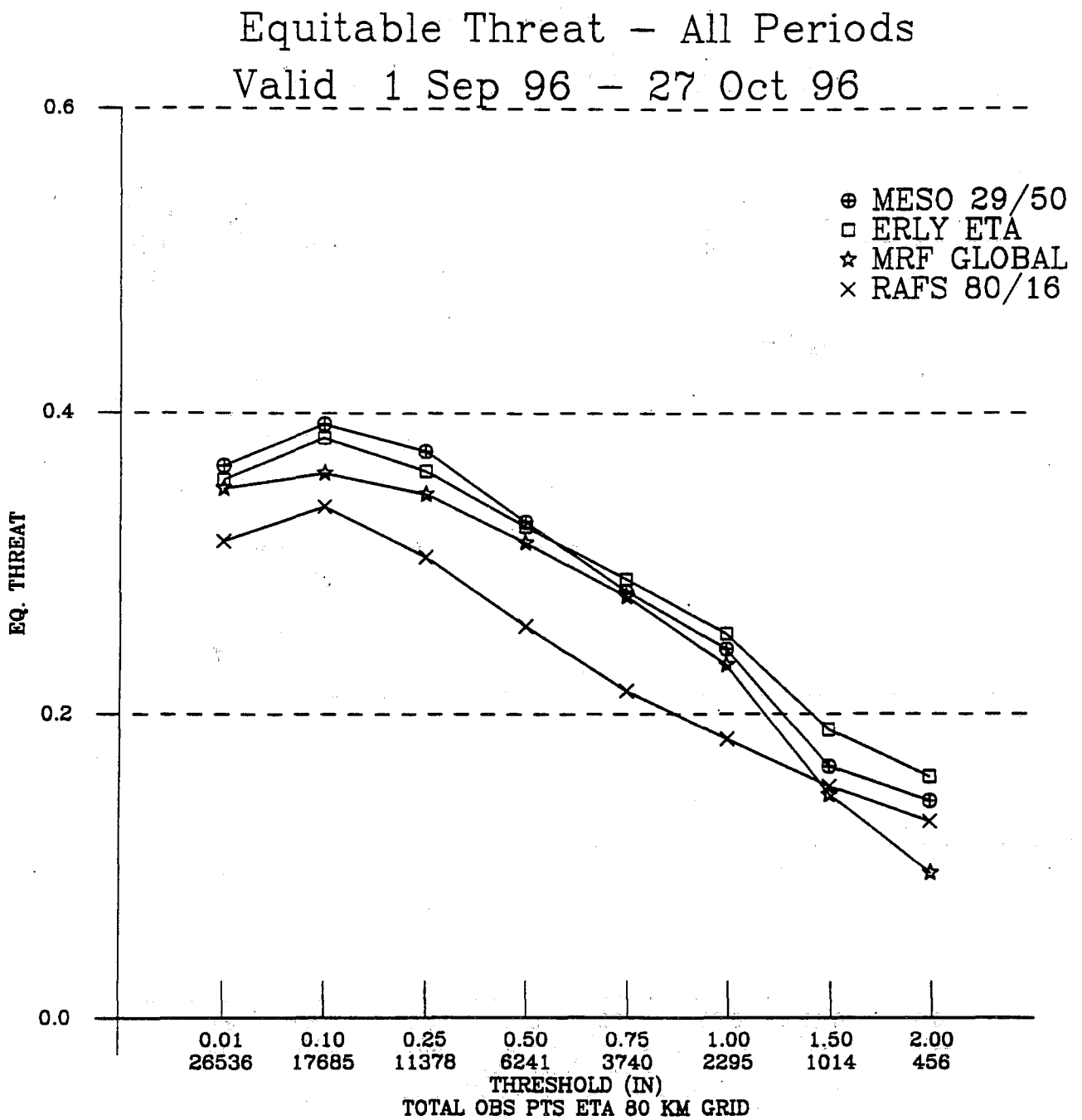

Figure 18: Equitable threat scores for all forecasts during the period 1 September - 27 October 1996.

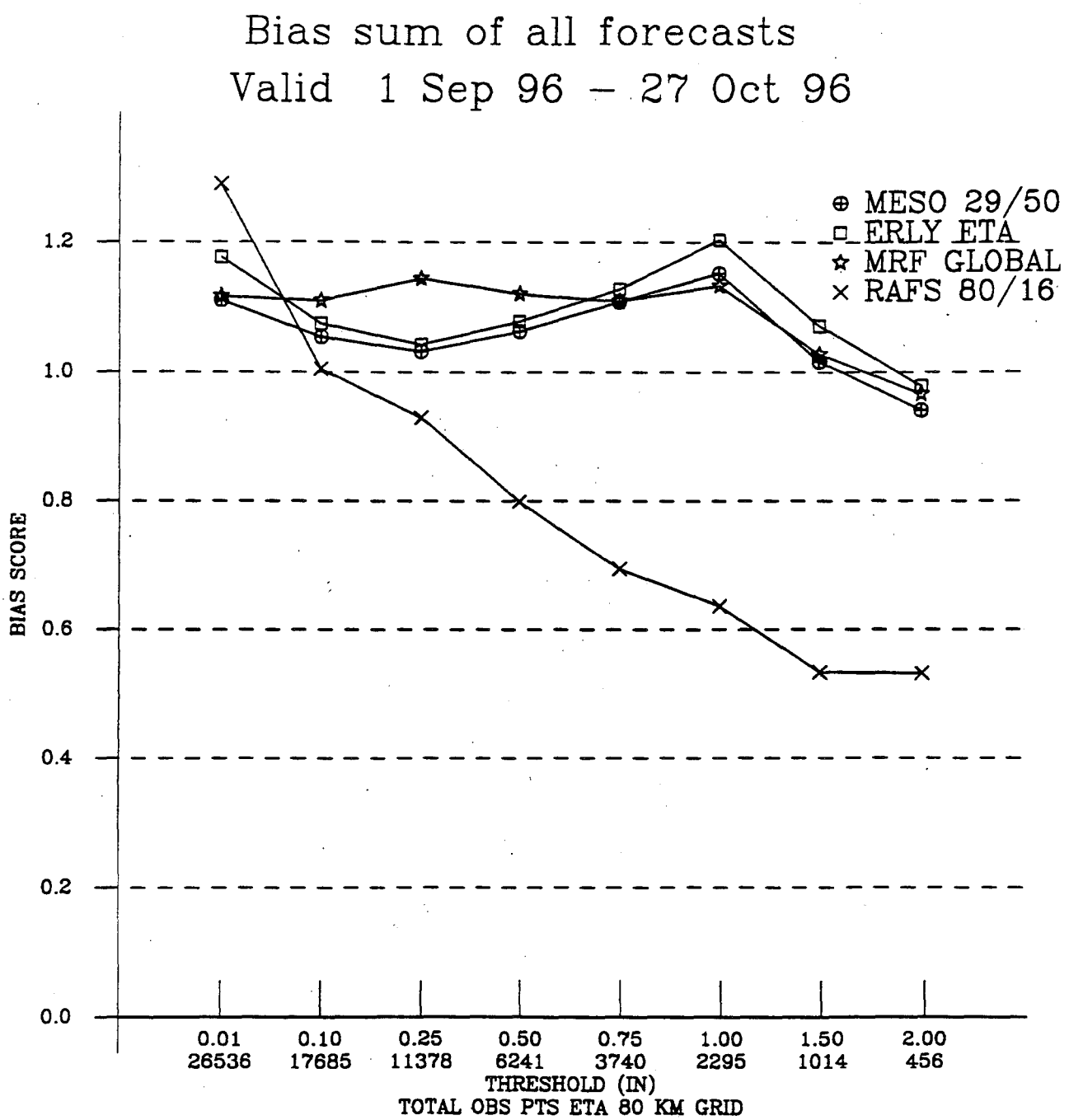

Figure 19: Bias sum scores for all forecasts during the period of 1 September - 27 October 1996.

144 Arizona Cool Season Climatological Surface Wind and Pressure Gradient Study. Ira S. Brenner, May 1979. (PB298900/AS)
146 The BART Experiment. Morris S. Webb, October 1979. (PB80 155112)
147 Occurrence and Distribution of Flash Floods in the Western Region. Thomas L. Dietrich, December 1979. (PB80 160344)
149 Misinterpretations of Precipitation Probability Forecasts. Allan H. Murphy, Sarah Lichtenstein, Baruch Fischhoff, and Robert L. Winkler, February 1980. (PB80 174576)
150 Annual Data and Verification Tabulation - Eastern and Central North Pacific Tropical Storms and Hurricanes 1979. Emil B. Gunther and Staff, EPHC, April 1980. (PB80 220486)
NMC Model Performance in the Northeast Pacific. James E. Overland, PMEL-ERL, April 1980. (PB80 196033)
Climate of Salt Lake City, Utah. William J. Alder, Sean T. Buchanan, William Cope (Retired), James A. Cisco, Craig C. Schmidt, Alexander R. Smith (Retired), Wilbur E. Figgins (Retired), April 1996 - Sixth Revision (PB96 175583)
153 An Automatic Lightning Detection System in Northern California. James E. Rea and Chris E. Fontana, June 1980. (PB80 225592)
154 Regression Equation for the Peak Wind Gust 6 to 12 Hours in Advance at Great Falls During Strong Downslope Wind Storms. Michael J. Oard, July 1980. (PB91 108367)
155 A Raininess Index for the Arizona Monsoon. John H. Ten Harkel, July 1980. (PB81 106494)
156 The Effects of Terrain Distribution on Summer Thunderstorm Activity at Reno, Nevada. Christopher Dean Hill, July 1980. (PB81 102501)
157 An Operational Evaluation of the Scofield/Oliver Technique for Estimating Precipitation Rates from Satellite Imagery. Richard Ochoa, August 1980. (PB81 108227)
158 Hydrology Practicum. Thomas Dietrich, September 1980. (PB81 134033)
159 Tropical Cyclone Effects on California. Arnold Court, October 1980. (PB81 133779)
160 Eastern North Pacific Tropical Cyclone Occurrences During Intraseasonal Periods. Preston W. Leftwich and Gail M. Brown, February 1981. (PB81 205494)
161 Solar Radiation as a Sole Source of Energy for Photovoltaics in Las Vegas, Nevada, for July and December. Darryl Randerson, April 1981. (PB81 224503)
162 A Systems Approach to Real-Time Runoff Analysis with a Deterministic Rainfall-Runoff Model. Robert J.C. Burnash and R. Larry Ferral, April 1981. (PB81 224495)
163 A Comparison of Two Methods for Forecasting Thunderstorms at Luke Air Force Base, Arizona. LTC Keith R. Cooley, April 1981. (PB81 225393)
164 An Objective Aid for Forecasting Afternoon Relative Humidity Along the Washington Cascade East Slopes. Robert S. Robinson, April 1981. (PB81 23078)
165 Annual Data and Verification Tabulation, Eastern North Pacific Tropical Storms and Hurricanes 1980. Emil B. Gunther and Staff, May 1981. (PB82 230336)
166 Preliminary Estimates of Wind Power Potential at the Nevada Test Site. Howard G. Booth, June 1981. (PB82 127036)
167 ARAP User's Guide. Mark Mathewson, July 1981, Revised September 1981. (PB82 196783)
168 Forecasting the Onset of Coastal Gales Off Washington-Oregon. John R. Zimmerman and William D. Burton, August 1981. (PB82 127051)
169 A Statistical-Dynamical Model for Prediction of Tropical Cyclone Motion in the Eastern North Pacific Ocean. Preston W. Leftwich, Jr., October 1981. (PB82195298)
170 An Enhanced Plotter for Surface Airways Observations. Andrew J. Spry and Jeffrey L. Anderson, October 1981. (PB82 153883)
171 Verification of 72-Hour 500-MB Map-Type Predictions. R.F. Quiring, November 1981. (PB82-158098)
172 Forecasting Heavy Snow at Wenatchee, Washington. James W. Holcomb, December 1981. (PB82-177783)
173 Central San Joaquin Valley Type Maps. Thomas R. Crossan, December 1981. (PB82 196064)
174 ARAP Test Results. Mark A. Mathewson, December 1981. (PB82 198103)
Approximations to the Peak Surface Wind Gusts from Desert Thunderstorms. Darryl Randerson, June 1982. (PB82 253089)
Climate of Phoenix, Arizona. Robert J. Schmidli and Austin Jamison, April 1969 (Revised July 1996). (PB96-191614)
178 Annual Data and Verification Tabulation, Eastern North Pacific Tropical Storms and Hurricanes 1982. E.B. Gunther, June 1983. (PB85 106078)
179 Stratified Maximum Temperature Relationships Between Sixteen Zone Stations in Arizona and Respective Key Stations. Ira S. Brenner, June 1983. (PB83 249904)
180 Standard Hydrologic Exchange Format (SHEF) Version I. Phillip A. Pasteris, Vernon C. Bissel, David G. Bennett, August 1983. (PB85 106052)
181 Quantitative and Spacial Distribution of Winter Precipitation along Utah's Wasatch Front. Lawrence B. Dunn, August 1983. (PB85 106912)
182 500 Millibar Sign Frequency Teleconnection Charts - Winter. Lawrence B. Dunn, December 1983. (PB85 106276)
183 500 Millibar Sign Frequency Teleconnection Charts - Spring. Lawrence B. Dunn, January 1984. (PB85 111367)
184 Collection and Use of Lightning Strike Data in the Western U.S. During Summer 1983. Glenn Rasch and Mark Mathewson, February 1984. (PB85 110534)
185 500 Millibar Sign Frequency Teleconnection Charts - Summer. Lawrence B. Dunn, March 1984. (PB85 111359)
186 Annual Data and Verification Tabulation eastern North Pacific Tropical Storms and Hurricanes 1983. E.B. Gunther, March 1984. (PB85 109635)
187 500 Millibar Sign Frequency Teleconnection Charts - Fall. Lawrence B. Dunn, May 1984. (PB85-110930)
188 The Use and Interpretation of Isentropic Analyses. Jeffrey L. Anderson, October 1984. (PB85-132694)
189 Annual Data & Verification Tabulation Eastern North Pacific Tropical Storms and Hurricanes 1984. E.B. Gunther and R.L. Cross, April 1985. (PB85 1878887AS)
190 Great Salt Lake Effect Snowfall: Some Notes and An Example. David M. Carpenter, October 1985. (PB86 119153/AS)
191 Large Scale Patterns Associated with Major Freeze Episodes in the Agricultural Southwest. Ronald S. Hamilton and Glenn R. Lussky, December 1985. (PB86 144474AS)
192 NWR Voice Synthesis Project: Phase I. Glen W. Sampson, January 1986. (PB86 145604/AS)
193 The MCC - An Overview and Case Study on Its Impact in the Western United States. Glenn R. Lussky, March 1986. (PB86 170651/AS)
194 Annual Data and Verification Tabulation Eastern North Pacific Tropical Storms and Hurricanes 1985. E.B. Gunther and R.L. Cross, March 1986. (PB86 170941/AS)
195 Radid Interpretation Guidelines. Roger G. Pappas, March 1986. (PB86 177680/AS)
196 A Mesoscale Convective Complex Type Storm over the Desert Southwest. Darryl Randerson, April 1986. (PB86 190998/AS)
197 The Effects of Eastern North Pacific Tropical Cyclones on the Southwestern United States. Walter Smith, August 1986. (PB87 106258AS)
198 Preliminary Lightning Climatology Studies for Idaho. Christopher D. Hill, Carl J. Gorski, and Michael C. Conger, April 1987. (PB87 180196/AS)
Heavy Rains and Flooding in Montana. A Case for Slantwise Convection. Glenn R. Lussky, April 87. (PB87 185229/AS)
Annual Data and Verification Tabulation Eastern North Pacific Tropical Storms and Hurricanes 1986. Roger L. Cross and Kenneth B. Mielke, September 1987. (PB88 110895/AS)
201 An Inexpensive Solution for the Mass Distribution of Satellite Images. Glen W. Sampson and George Clark, September 1987. (PB88 114038/AS)
202 Annual Data and Verification Tabulation Eastern North Pacific Tropical Storms and Hurricanes 1987. Roger L. Cross and Kenneth B. Mielke, September 1988. (PB88-101935/AS)
203 An Investigation of the 24 September 1986 "Cold Sector" Tornado Outbreak in Northern California. John P. Monteverdi and Scott A. Braun, October 1988. (PB89 121297/AS)
204 Preliminary Analysis of Cloud-To-Ground Lightning in the Vicinity of the Nevada Test Site. Carven Scott, November 1988. (PB89 128649/AS)
205 Forecast Guidelines For Fire Weather and Forecasters -- How Nighttime Humidity Affects Wildland Fuels. David W. Goens, February 1989. (PB89 162549/AS)
206 A Collection of Papers Related to Heavy Precipitation Forecasting. Western Region Headquarters, Scientific Services Division, August 1989. (PB89 230833/AS)
207 The Las Vegas McCarran International Airport Microburst of August 8, 1989. Carven A. Scott, June 1990. (PB90-240268)
208 Meteorological Factors Contributing to the Canyon Creek Fire Blowup, September 6 and 7, 1988. David W. Goens, June 1990. (PB90-245085)
209 Stratus Surge Prediction Along the Central California Coast. Peter Felsch and Woodrow Whitlatch, December 1990. (PB91-129239)
210 Hydrotools. Tom Egger. January 1991. (PB91-151787/AS)
211 A Northern Utah Soaker. Mark E. Struthwolf, February 1991. (PB91-168716)
212 Preliminary Analysis of the San Francisco Rainfall Record: 1849-1990. Jan Null, May 1991. (PB91-208439)
213 Idaho Zone Preformat, Temperature Guidance, and Verification. Mark A. Mollner, July 1991. (PB91-227405/AS)
214 Emergency Operational Meteorological Considerations During an Accidental Release of Hazardous Chemicals. Peter Mueller and Jerry Galt, August 1991. (PB91-235424)
215 WeatherTools. Tom Egger, October 1991. (PB93-184950)
216 Creating MOS Equations for RAWS Stations Using Digital Model Data. Dennis D. Gettman, December 1991. (PB92-131473/AS)
217 Forecasting Heavy Snow Events in Missoula, Montana. Mike Richmond, May 1992. (PB92-196104)
218 NWS Winter Weather Workshop in Portland, Oregon. Various Authors, December 1992. (PB93-146785)
219 A Case Study of the Operational Usefulness of the Sharp Workstation in Forecasting a Mesocyclone-Induced Cold Sector Tornado Event in California. John P. Monteverdi, March 1993. (PB93-178697)
220 Climate of Pendleton, Oregon. Claudia Bell, August 1993. (PB93-227536)
221 Utilization of the Bulk Richardson Number, Helicity and Sounding Modification in the Assessment of the Severe Convective Storms of 3 August 1992. Eric C. Evenson, September 1993. (PB94-131943)
222 Convective and Rotational Parameters Associated with Three Tornado Episodes in Northern and Central California. John P. Monteverdi and John Quadros, September 1993. (PB94-131943)
223 Climate of San Luis Obispo, California. Gary Ryan, February 1994. (PB94-162062)
224 Climate of Wenatchee, Washington. Michael W. McFarland, Roger G. Buckman, and Gregory E. Matzen, March 1994. (PB94-164308)
225 Climate of Santa Barbara, California. Gary Ryan, December 1994. (PB95-173720)
226 Climate of Yakima, Washington. Greg DeVoir, David Hogan, and Jay Neher, December 1994. (PB95-173688)
227 Climate of Kalispell, Montana. Chris Maier, December 1994. (PB95-169488)
228 Forecasting Minimum Temperatures in the Santa Maria Agricultural District. Wilfred Pi and Peter Felsch, December 1994. (PB95-171088)
229 The 10 February 1994 Oroville Tornado--A Case Study. Mike Staudenmaier, Jr., April 1995. (PB95-241873)
230 Santa Ana Winds and the Fire Outbreak of Fall 1993. Ivory Small, June 1995. (PB95-241865)
231 Washington State Tornadoes. Treste Huse, July 1995. (PB96-107024)
232 Fog Climatology at Spokane, Washington. Paul Frisbie, July 1995. (PB96-106604)
233 Storm Relative Isentropic Motion Associated with Cold Fronts in Northern Utah. Kevin B. Baker, Kathleen A. Hadley, and Lawrence B. Dunn. July 1995. (PB96-106596)
234 Some Climatological and Synoptic Aspects of Severe Weather Development in the Northwestern United States. Eric C. Evenson and Robert H. Johns, October 1995. (PB96-112958)
235 Climate of Las Vegas, Nevada. Paul H. Skrbac and Scott Cordero, December 1995. (PB96-135553)
236 Climate of Astoria, Oregon. Mark A. McInerney, January 1996.
237 The 6 July 1995 Severe Weather Events in the Northwestern United States: Recent Examples of SSWEs. Eric C. Evenson, April 1996.
238 Significant Weather Patterns Affecting West Central Montana. Joe Lester, May 1996. (PB96-178751)
239 Climate of Portland, Oregon. Clinton C. D. Rocky, May 1996. (PB96-17603)
240 Downslop Winds of Santa Barbara, CA. Gary Ryan, July 1996 (PB96-191697)
241 Operational Applications of the Real-time National Lightning Detection Network Data at the NWSO Tucson, AZ. Darren McCollum, David Bright, Jim Meyer, and John Glueck, September 1996. (PB97-108450)
242 Climate of Pocatello, Idaho. Joe Heim, October 1996. (PB97-114540)
243 Climate of Great Falls. Montana. Matt Jackson and D. C. Williamson, December 1996. (PB97-126684)
244 WSR-88D VAD Wind Profile Data Influenced by Bird Migration over the Southwest United States. Jesus A. Haro, January 1997. (PB97-135263)
245 Climatology of Cape for Eastern Montana and Northern Wyoming. Heath Hockenberry and Keith Meier, January 1997. (PB97-133425)

NOAA SCIENTIFIC AND TECHNICAL PUBLICATIONS

The National Oceanic and Atmospheric Administration was established as part of the Department of Commerce on October 3, 1970. The mission responsibilities of NOAA are to assess the socioeconomic impact of natural and technological changes in the environment and to monitor and predict the state of the solid Earth, the oceans and their living resources, the atmosphere, and the space environment of the Earth.

The major components of NOAA regularly produce various types of scientific and technical information in the following kinds of publications.

PROFESSIONAL PAPERS--Important definitive research results, major techniques, and special investigations.

CONTRACT AND GRANT REPORTS--Reports prepared by contractors or grantees under NOAA sponsorship.

ATLAS--Presentation of analyzed data generally in the form of maps showing distribution of rainfall, chemical and physical conditions of oceans and atmosphere, distribution of fishes and marine mammals, ionospheric conditions, etc.

TECHNICAL SERVICE PUBLICATIONS -- Reports containing data, observations, instructions, etc. A partial listing includes data serials; prediction and outlook periodicals; technical manuals, training papers, planning reports, and information serials; and miscellaneous technical publications.

TECHNICAL REPORTS--Journal quality with extensive details, mathematical developments, or data listings.

TECHNICAL MEMORANDUMS--Reports of preliminary, partial, or negative research or technology results, interim instructions, and the like.

Information on availability of NOAA publications can be obtained from:

NATIONAL TECHNICAL INFORMATION SERVICE

U. S. DEPARTMENT OF COMMERCE

5285 PORT ROYAL ROAD

SPRINGFIELD, VA 22161